PEOPULE'S DEMOCRATIC REPUBLIC OF ALGERIA

Higher Education and Scientific Research Ministry

University of El-oued
Faculty of Sciences and Technology

N° d'ordre :
N° de série :

A Dissertation Submitted to the Department of Physics

In Partial Fulfillment of the Requirements

For the Degree of Master in

Applied Physics Radiation and Energy

by**: Khaoula KHELAIFA**

Title

Structural and opto-electrical study of SnO_2 thin films elaborated by spray pyrolysis (home made)

Discussed on 10/06/2015

Members of jury:

Mosbah DIFALLAH	MCA	University of El-Oued	President
Fethi BOURAS	MCA	University of El-Oued	Examiner
Achour RAHAL	MAA	University of El-Oued	Examiner
Boubaker BENHAOUA	Pr	University of El-Oued	Supervisor

University season: 2015/2014

Dedication

I dedicate this modest work to my dear
Mother and Father

To my husband

To all my family brother and sisters

All my cousins

To all my classmates

Acknowledgements

I thank God who give me the patience to finich this work

My parent for their support

My supervisor Dr. Boubaker BENHAOUA, for the useful comments, remarks and engagement through the learning process of this master thesis

And I would like to thank the jury for their acceptance to examine this work

And sincere thanks to each of the characters taught me I became a slave to him.

khaoula

Table of Contents

Chapter I: Transparent Conductive Oxides (TCOs)

Chapter II: Thin Film Deposition Methods

Chapter III: Characterizations methods and experimental

Chapter IV: Results and Discussion

List of Figure

Chapter I: Transparent Conductive Oxides (TCOs)

Chapter II: Thin Film Deposition Methods

Chapter III: Characterizations Methods and Experimental

Chapter IV: Results and Discussion

List of Table

Chapter I: Transparent Conductive Oxides (TCOs)

Chapter II: Thin Film Deposition Methods

Chapter III: Characterizations Methods and Experimental

Chapter IV: Results and Discussion

Nomenclature

Romane Symbols

N	The number of charge carriers (cm^{-3})
μ	The mobility of charge carriers ($cm^2.V^{-1}.S^{-1}$)
e	Electronic charge
τ	The relaxation time
m^*	The effective mass of the charge carrier
λ_{mfp}	Mean free path of these charge carriers
V_F	The drift velocity
a_0^*	The effective Bohr radius
ε^m	The static dielectric constant
m_c^*	The effective mass of the electrons in the conduction band
ε_0	Vacuum permittivity
h	Planck constant.
$\hbar$	The reduced Planck constant
k	The wave vector
c	The speed of light (3.10^8 m/s)
R	The zero degree incidence reflectance
d	The film thickness
α	The absorption coefficient
k	The extinction coefficient
$h\nu$	The photon energy
ν	Electromagnetic wave frequency
T	The transmittance
Rs	The sheet resistance
E_u	Urbach energy
ρ	The volume resistivity ($\Omega.cm$)
V	The measured voltage (volts)
I	The source current (amperes)
d	The sample thickness (cm)
d_{hkl}	Inter-planer spacing
θ	The Bragg angle

n	The order of the spectrum;
λ	The wavelength of X-rays
D	The crystallite size
β	The full width at half maxima of the peak (FWHM) in radians
a, c	Tthe lattice parameters

Greek Symbol

TCOs	Transparent Conductive Oxides
CdO	Cadmium oxide
SnO_2	Tin oxide
ZnO	Zinc oxide
Sb	Antimony
ATO	Antimony doped Tin oxide
TiO_2	Titan oxide
In_2O_3	Indium oxide
CVD	Chemical Vapor Deposition
PVD	Physical Vapor Deposition
MOCVD	Metal-organic CVD
PECVD	Photo-Enhanced Chemical Vapor Deposition
LCVD	Laser-Induced Chemical Vapor Deposition
PECVD	Plasma-enhanced CVD
XRD	X-Ray Diffraction
UV/Vis	ultraviolet/visible

General Introduction

General Introduction

Every solid object has a surface, this surface is the discontinuity in the properties of the bulk materials and has been the target of modifications (artistic decoration and/or functional improvement) since the earliest times of mankind [1].

Today, modern products offer even more new functions with the unusual properties that often cannot be found in bulk sample. These product materials open completely new areas of applications. The multifunctionality of these technical products especially concerns their surface properties. Surface coating of glass with different types of films is one of the technologies that occupy a key position in the material and product development. Transparent Conducting Oxide (TCO) thin films are deposited on transparent substrates to form transparent electrodes [3]. Transparent electrodes is the key component of a variety cutting-edge applications, such as solar cells, gas sensors, organic light-emitting diodes, liquid crystal displays, electrochromic smart windows, as well as architectural coatings.

All TCOs can be classified into two major classes; the p-type and the n-type, on the basis of their majority charge carriers. However, the n-type TCOs are the most readily available and therefore more commonly found in practical applications. TCOs have a wide variety of industrial and commercial applications. Their ability to reflact thermal infrared heat is exploited to make energy-conserving windows. These low emissivity windows are the largest area of current use for TCOs. Oven windows employ TCOs to conserve energy and to maintain an outside temperature that makes them safe to touch. Microwaves windows are coated with TCO which allows visible light to pass and block microwaves so as to protect eyes [4].

Deposition of high quality, uniform thin films, is an intensive area of research which has yielded many varied deposition techniques each technique falls into one of three broad categories: wet chemical deposition; physical vapor deposition and chemical vapor deposition. Careful selection of the appropriate deposition technique is essential for control over the properties of the resultant films. Different techniques can affect growth rates, crystalline [5].

The first TCO material was reported in 1907 when K.Badeker sputter coated a thin film of cadmium and heat treated the sample in air [6]. Current TCO materials include tin-doped indium oxide In_2O_3:Sn (ITO) [7], fluorine doped tin oxide SnO_2:F (FTO) [8] and aluminum doped zinc oxide ZnO:Al (AZO) [9]. These materials, instead of relying on intrinsic vacancies within the metal oxide structure, These drawbacks have led to the development of fluorine-doped tin oxide, antimony-doped tin oxide [10], which is studied in this work.

In this work, I will try to stapes in writing this memory as follow:

* The first chapter includes the transparent conductive oxides and its important properties. We chose one of them which our study in this work is. It's the tin oxide (SnO_2).

* The second chapter I used some methods to get the thin film deposited in good way. We will focus on the techniques spray pyrolysis which is the support of research laboratory.

* The third chapter is introductions of the experimentally part in which we will study some reviews methods that used define the electrical optical and structural properties of the thin films. In addition the experimental methods used in preparing and getting the doped and undoped thin films takes place in this context.

* In the fourth and the last chapter we will explain and analyze the obtained results and give a general conclusion on it.

Reference of General Introduction

[1] **Afzal. Khan** , "Synthèse de Cuprates de Strontium ($SrCu_2O$) par MOCVD comme couche mince d'oxyde transparent conducteur de type P", Thése Pour obtenir le grade de Docteur de L'unversite de grenoble, (7 août 2006).

[2] **H. Bach and D. Krause.** "Thin Films on Glass. Springer-Verlag", Berlin, (2003).

[3] **Zhigang R. Li and Hong Meng**, "Organic Light-emitting Materials and Devices". CRC Press, USA, (2007).

[4] **B. O'Neill,** "Indium: Supply, Demand and Flat Panel Displays, Presented at Minor Metals", London, (June 2004) .

[5] **Dedova. Tatjana. PhD**, "Chemical spray pyrolysis deposition of Zink sulfide Thin Film and Zink Oxide Nanostructured Layers", Volume 20, (2009).

[6] **K. Baedeker**, Ann. Phys, 22:749–766, (1907).

[7] **G.Rupprecht,** Z.Phys (1954), 139, 504.

[8] **B. Benhaoua, S. Abbas, A. Rahal, A. Benhaoua, M.S. Aida,** "Effect of film thickness on the structural, optical and electrical properties of SnO: F thin films prepared by spray ultrasonic for solar cells applications", Superlattices and Microstructures 83 (2015) 78–88.

[9] **K. L. Menouer**, "Etude et réalisat ion d'une cellule solaire multicouches du type Si-SiO_2-SnO_2-ZnO par APCVD", thèse de doctorat, Université Mouloud Mammeri de TIZIOUZOU,(2011).

[10] **A. Rahal, A. Benhaoua, Ch. Bouzidi, B. Benhaoua, B. Gasmi,** "Effect of antimony doping on the structural, optical and electrical properties of SnO_2 thin films prepared by spray ultrasonic", Superlattices and Microstructures 76 (2014)105–114.

Chapter I

Transparent Conductive Oxides (TCOs)

Transparent Conductive Oxides (TCOs)

Based on Electromagnetic Theory (Maxwell's equations), which could not permit a material to be both electrically conducting and optically transparent simultaneously. Optically transparent materials tend to be electrical insulators by virtue of their large band gaps. However, Transparent Conductive Oxides (TCOs) is a group of materials with unique optoelectrical properties. Among different TCOs, Zinc oxide films, Indium oxide and tin oxide which will study in this work.

I.1. Transparent Conductive Oxides

A metal oxide in the thin film form transparent to visible light and conducting to electricity is called a transparent conducting oxide (TCO) [1]. The TCO semiconductors suitable for transparent electrodes should have a band gap energy approximately above 3.1 eV (i.e., degenerate n-type or p-type semiconductors) [11,12]. Transparent conductive oxides (TCO) are materials that exhibit a low resistivity of the order of 10^{-4} (Ω.cm), and high carrier concentration in the range $(0.1\text{-}1.0)x10^{21}$ cm^{-3} while being transparent in the visible part of the electromagnetic spectrum, typically having an average visible transmittance of 80% [13,14].

In our daily lives transparent conducting oxide (TCO) materials are used in numerous devices. These applications are mostly found in display technology [4], (organic) light-emitting-diodes (OLEDs) [15], thin-film solar photovoltaic [8], and smart windows [16].

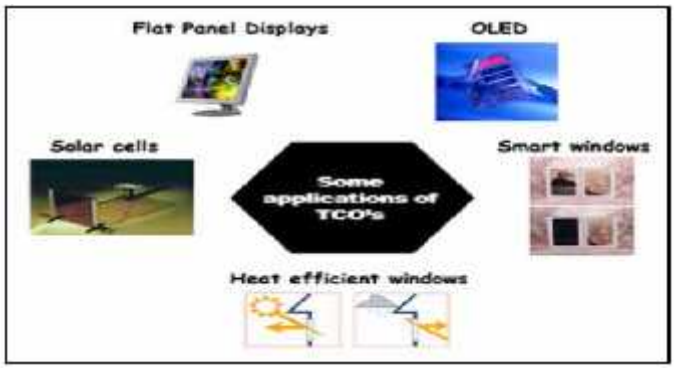

Figure (I-1): Some applications of TCOs [16].

I.2. Historical Background

The history of TCO starts from 1907, with the discovery of Cadmium Oxide (CdO), in thin film form, by a German scientist Karl Baedeker [6]. The first TCO patents for undoped and doped tin oxide (SnO_2) films were filed respectively in 1931 and 1942 [17,18]. Later, a practical

use of TCO started with discovery of tin-doped In_2O_3 in 1954 by G. Rupprecht [9]. In 1960s, it was recognized that thin films composed of binary compounds such as SnO_2, ZnO, In_2O_3 and their alloys are also good TCOs [1]. In 1980s, impurity-doped ZnO. In 1990s, new TCO materials consisting of multicomponent oxides, SnO_2 and ZnO, have been developed [1]. Among all these TCO materials the tin-doped indium oxide commonly known as indium tin oxide (ITO) [19]. All these TCOs have electrons as majority charge carriers and hence known as n-type TCOs. In 1993, develop p-type TCOs is thus an undeniable fact until now so many p-type TCOs have been reported after NiO as a first p-type TCO [20]. However, $SrCu_2O_2$ has been found a promising candidate for p-type TCOs because of its direct band gap and due to the fact that it can be deposited at relatively low temperature [20]. However, until now no efficient p-type TCO having optoelectrical properties comparable to its n-type counterpart is available.

I.3. TCOs Properties

In general, a TCO must exhibit three important qualities: high optical transparency, good electrical conductivity and mechanical durability including flexibility [21] some of the most relevant properties of a TCO are:

I.3.1. Electrical properties

TCOs are wide band gap semiconducting oxides, with high conductivity in the range 10^{-9}_10^{5} ($S.cm^{-1}$) [22,23]. TCOs may be n or p-type semiconductors depending up on their charge carrier generation mechanism.

*** Electrical conductivity**

The conductivity is a product of the number of charge carriers in a material, and the mobility of these charge carriers, times the elementary electron charge. The electrical conductivity $\sigma(\Omega^{-1}cm^{-1})$ is given by [22]:

$$\sigma = n \,.\mu \,.e = {}^{1}/_{\rho} \qquad (I-1)$$

The resistivity ρ is defined as the inverse of the conductivity.

where n: The number of charge carriers (cm^{-3}).

μ : The mobility of charge carriers ($cm^2.V^{-1}.S^{-1}$).

e : Electronic charge.

For thin films of uniform thickness ***d***, the electrical resistance is sometimes expressed as the sheet resistance ***Rs*** **(**$\Omega.cm^{-2}$) is written by [22]:

$$Rs = {}^{\rho}/_{d} \qquad (I-2)$$

Other than the thickness, the sheet resistance is independent of the film dimensions.

The conductivity of TCOs is reflected from the mobility, that can be expressed as [24]:

$$\mu = \frac{e.\tau}{m^*} = \frac{e.\lambda_{mfp}}{m^*.V_F} \qquad (I-3)$$

where τ: The relaxation time;

m^*: The effective mass of the charge carrier;

λ_{mfp}: Mean free path of these charge carriers;

V_F: The drift velocity.

The conductivity of n-type TCOs is always higher than that of p-type due to relative small effective mass of electron in conduction band than that of hole in the valence band [1].

***Band gap and doping of TCOs**

In order to promote conductivity, the number of charge carriers can be increased by doping. Dependant on the material this can be done by substitutional doping, creation of vacancies or implantation of interstitials. Dependant on the valence of dopants or vacant sites, acceptor or donor states will induce p- or n-type conductivity [25]. The range of Eg for different dopants is shown in the Table (I-1).

Table (I-1): The range of Eg for different dopants.

TCOs		Eg	Dopants	Reference
n	SnO_2	3.6 – 4.2	Sb, F, Fe, Nb, Pd, In, Co	[26]
	ZnO	3.2 – 3.3	Al, Ga, B, In, F, Si, Ge,	[27]
	In_2O_3	3.5– 3.75	Sn, Ge, Mn, Fe,Ti, Nb, Ta	[7]
P	$SrCu_2O_2$	~3.3	K, Ba, Ca, CaO	[1]
	NiO	3.11	Li, Na, Fe, B, Al	[28]
	$CuAlO_2$	3.5	Mg, Mn, Ca, Zn	[29]

The presence of a band gap, providing low absorption in the visible range, is an essential feature of TCOs. Metal-oxide semiconductors having a band gap more than 3 eV meet this

condition. The top of the valence band (B_V) is mostly formed by the oxygen **2p** bands, whereas the bottom of the conduction band (B_C) is composed of a single and highly dispersed metal **s** band. The Oxygen 2p orbitals are low in energy and that it is a large band gap (Eg) can be obtained in oxides [25]. The band structure of metal-oxide (SnO_2) is described in Figure (I-2).

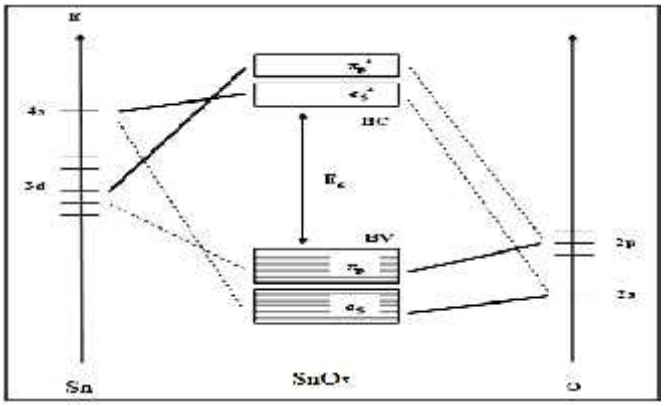

Figure (I-2): Schematic for structure of SnO_2 [30].

In intrinsic stoichiometric oxides, coexistence of electrical conductivity besides visible transparency is not possible. However, substitutional doping by cationic donors or anion vacancies can create charge carriers, i.e. electrons. The donor (or acceptor) states alter the electronic band structure of the material. For increased donor density, the donor states merge with the conduction band at a certain critical density n_c, whose magnitude can be estimated by Mott's criterion [25].

$$n_c^{1/3}.a_0^* \approx 0.25 \qquad (I-4)$$

The effective Bohr radius a_0^* is given by:

$$a_0^* = \frac{h^2.\varepsilon_0.\varepsilon^m}{\pi.e^2.m_c^*} \qquad (I-5)$$

where ε^m: The static dielectric constant;

m_c^*: The effective mass of the electrons in the conduction band;

ε_0: Vacuum permittivity;

h: Planck constant.

In general, the carrier density in TCOs is far larger than this ($\sim 10^{21} cm^{-3}$). Above this Mott critical density, free electron behavior can be expected. The donor states have merged with the conduction band and the material is said to be degenerate. The Fermi energy E_F is determined by the highest occupied state of the conduction band, and one can write [25]:

$$E_F = \frac{\hbar^2 k^2}{2m_c^*} \qquad (I-6)$$

where $\hbar$: The reduced Planck constant;

k: The wave vector.

The band structure of tin oxide is approximated by parabolic functions of **k** close to the band edges. The schematic representation in figure (I-3) is valid for most binary metal oxide wide band gap semiconductors. The valence band maximum and conduction band minimum are both located at k=0.

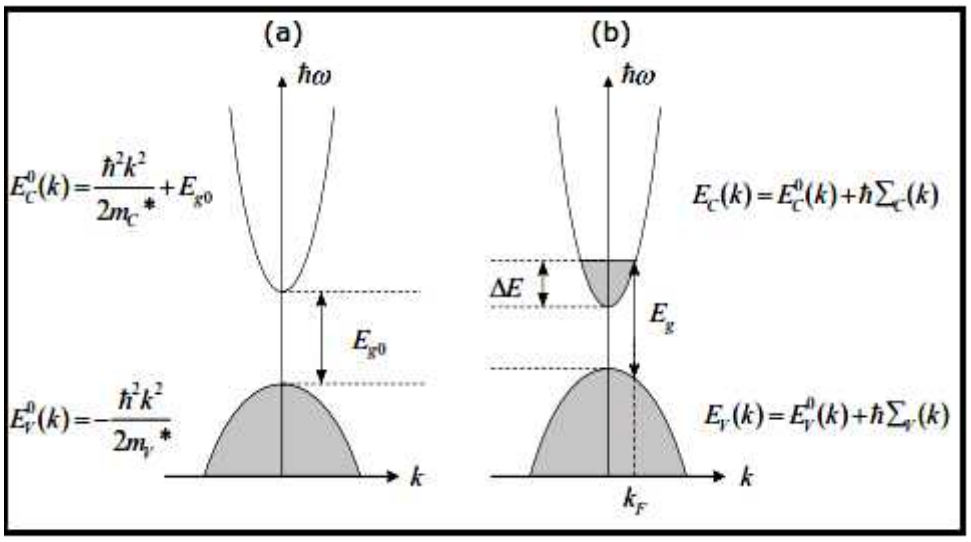

Figure (1-3): Schematic representation of the band structure of undoped (a) and doped (b) metal oxide wide band gap semiconductor in the vicinity of the top of the valence band and bottom of the conduction band [25].

I.3.2. Optical properties of TCOs

An important feature of TCOs is the existence of a transmission window covering most part of the visible spectrum. In literature, the optical transmission is defined as the ratio between incoming light intensity and transmitted intensity averaged over all values in between 300 nm and 800 nm [30]. The typical spectral dependence of TCOs is schematically shown in figure (I-4).

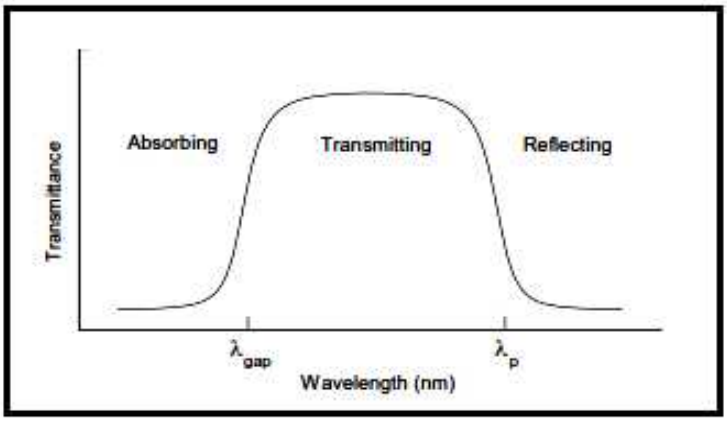

Figure (I-4): Spectral dependence of conducting transparent materials: λ_{gap} and λ_p are the wavelengths at which the band gap absorption and free electron plasma absorption takes place [31].

Transmission window is defined by two regions where no light is transmitted due to different phenomena.

- Low wavelengths ($\lambda<\lambda_{gap}$): the absorption due to the fundamental band gap dominates. The photon energy in this near-and deep-UV part of the spectrum is high enough to equal the band gap energy (3 – 4 eV). This energy is absorbed and transformed to band to band transitions, and no light is transmitted because of this quantum phenomenon.

- Longer wavelengths ($\lambda>\lambda_p$): in the (near) infrared (IR) part of the spectrum no light is transmitted due to the plasma edge. Here the light is electronically reflected which can be best described by the classical Drude free electron theory [31,32].

In the free electron model, the electrons may be thought of as plasma whose density is set into motion by the electric field component of the electromagnetic field. The plasma oscillates at a natural frequency $\boldsymbol{\omega_p}$, the resonance or plasma frequency. This frequency corresponds to the plasma wavelength $\boldsymbol{\lambda_p}$ and is of the order of (1 – 4 µm) for TCOs [28]. The plasma wavelength is written by [33]:

$$\lambda_P = \frac{2\pi c}{\omega_P} \qquad (I-7)$$

where c: The speed of light (3.10^8 m/s).

The TCO behaves like a dielectric and is transparent in the region for ($\omega>\omega_p$). In this transparent regime the film is weakly absorbing and the transmission can be expressed as [34]:

$$T = (1 - R)\exp(-\alpha d) \qquad (I - 8)$$

where R: The zero degree incidence reflectance;

d: The film thickness;

α: The absorption coefficient is dependent on the wavelength according to [33]:

$$\alpha = \frac{4\pi k}{\lambda} \qquad (I - 9)$$

where k: the extinction coefficient determine the absorptance of the material.

Close to λ_{gap} the reflectance is zero and the absorption coefficient as a function of wavelength can be obtained easily from the transmission curve. The following relation applies for direct allowed transitions [35]:

$$(\alpha h\nu) \propto \sqrt{h\nu - E_g} \qquad (I - 10)$$

where $h\nu$: The photon energy;

ν: Electromagnetic wave frequency.

The band gap energy is calculated from the Tauc plot [35], versus the photon energy $h\nu$. If $(\alpha h\nu)^2$ is extrapolated to the x-axis intersection ($(\alpha h\nu)^2$=0), formula (I-10) implies that the photon energy equals the band gap energy ($h\nu \approx Eg$). This method is commonplace to extract band gap energies from transmission data. Figure (I-5) shows the Tauc plot.

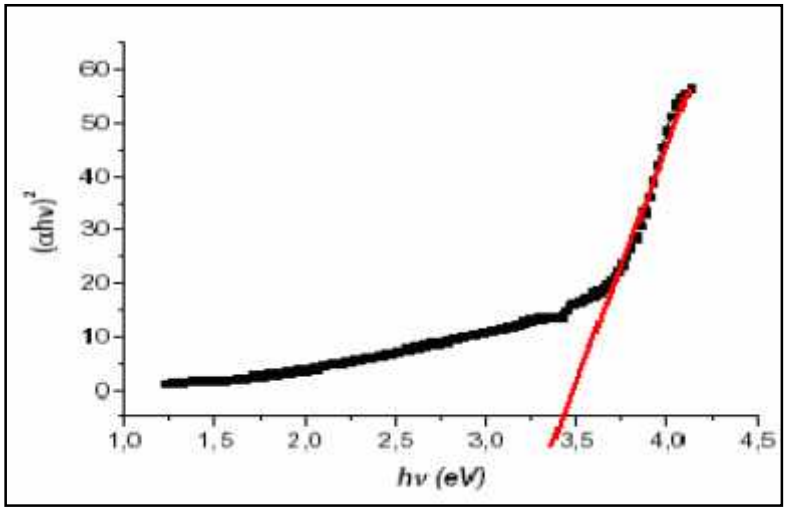

Figure (I-5): The band gap energy for SnO_2 film [9].

I.3.3. Electrical and optical correlation properties of TCOs

In many applications requiring transparent conducting films, the optical transmission and electrical conductivity should be as high as possible. This is particularly important for solar cell applications because high optical transmission in the visible region enhances the photo generated current and low sheet resistance (i.e. high electrical conductivity) reduces series resistance of the cell. The performance of transparent conductors is often assessed through figures of merit $\Phi(\Omega^{-1})$ which incorporate both electrical and optical parameters [36,37]. Figure of merit is calculated by using Haacke formula [38]:

$$\Phi = \frac{T^{10}}{Rs} \qquad (I-11)$$

where T: The transmittance;

Rs: The sheet resistance.

Both transmittance and resistivity were significantly affected by the film thickness. Figure of merit was used to determine the thickness at which the films present the best condition for their use in solar cells as widow and collector. Table (I-2) shows different values, of transmittance and conductance of thin films with different method deposition, which will be study in the chapter II.

Table (I-2): opto-electrical properties of different TCOs [25].

TCOs		σ ($\Omega^{-1}cm^{-1}$)	T(%)	Method deposition
n	SnO_2:Sb	1000	85	Spray
	ZnO:Al	3000	85	CVD
	In_2O_3	5000	86	PLD
P	$CuAlO_2$	2.94	70	PLD
	$SrCu_2O_2$	20.8	75	PLD

I.4. Tin oxide

Tin oxide (i.e. SnO_2), also known as stannic oxide, is a widely applied and studied as ceramic material [39]. SnO_2 belongs to the important class of transparent conductor oxide materials; it was the first to be TCO marketed that combine high optical transparency in the visible range of the electromagnetic spectrum and very good electrical conductivity [39]. Tin

oxide thin films are n-type semiconductors. They have a high band gap of **E**g = 3.6 - 4.2 eV [40,41], when suitably doped can be used both as n-type semiconductor.

I.4.1. Crystalline structure

Tin oxide has a single stable phase at ambient pressure [42], called cassiterite and adopts a square mesh rutile. Its space group P4/mnm. The unit cell has the parameters [9]:

$$a = b = 0.475 \text{ nm} \qquad \text{and} \qquad c = 0.318 \text{ nm}$$

And contains six atoms. Each tin ion, Sn^{4+} is at the center of an almost regular octahedron formed by six ions oxygen, O^{2-}, while each O^{2-} is surrounded by three-Sn^{4+} situated at the vertices of a triangle isosceles. The ionic radii of the cation Sn^{4+} and the anion O^{2-} have the values respectively 0.071 and 0.14 nm. A schematic representation of a unit cell oxide tin is reported in Figure (I-6).

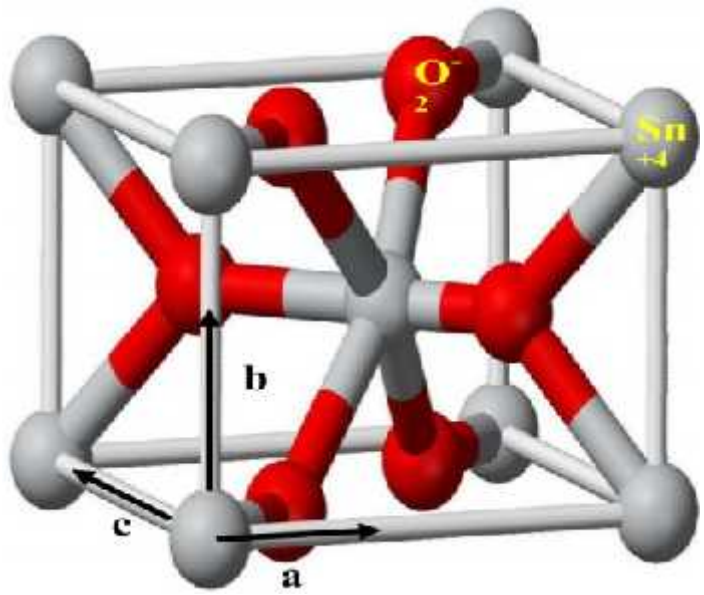

Figure (I-6): Unit cell of SnO_2 in the rutile structure [11].

I.4.2. SnO_2 gap

Tin oxide thin film gap varies between 3.6 and 4.2eV, its variations are related to the deposition techniques. Tin oxide gap is direct type. The extreme of the valence band and the conduction band are on the same axis of $\vec{k}$ vectors in the Brillouin zone. Electrons transitions from the valence band to the conduction band are vertically [9].

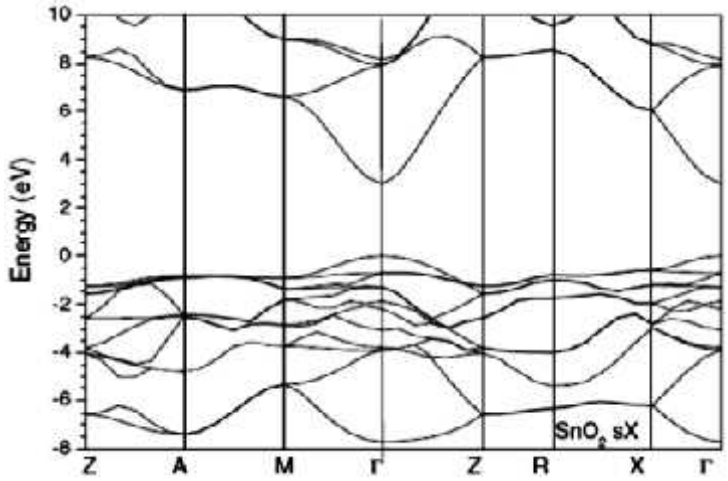

Figure (I-7): SnO_2 Band structure [9].

I.4.3. Electrical properties

Tin oxide (SnO_2), close to perfectly stoichiometry condition, have low free carrier concentration and high resistivity ($\rho \sim 10^8\ \Omega.cm$), which is similar to insulation. However, non-stoichiometric forms of these oxide films have high free carrier concentration between 10^{18} and $10^{20}\ cm^{-3}$. In other words, during crystal growth, there is an oxygen vacancy in the structure and therefore the formula for thin film form of this material is SnO_{2-x}, where x is the deviation from stoichiometry. Indeed, the electrical conduction in this material results from existence of defects in the crystal, generally, either oxygen vacancies or interstitial atoms, which may act as donor. It is possible to increase the free electron concentration or n-type conductivity in SnO_2 film, two important donors for tin oxides are F and Sb, which can increase the n-type electrical conductivity to several orders. F^{1-} substitutes O^{2-} with a free electron injected in B_c and Sb^{5+} substitutes Sn^{4+} so that an extra electron enters the lattice [10].

I.4.4. Optical properties

SnO_2 transparent conducting thin films are n-type semiconductors with a direct optical band gap about 3.6 – 4.2 eV**.** It has a high reflection of solar radiation in the range of infrared and strong absorption in the ultraviolet range, while it has a transmission of the order of 85% in the visible range and it becomes opaque beyond of 1200 nm. This reduction in optical transmission is due to the strong increase of absorption caused by the presence of free electrons [43]; as it will be seen in chapter IV.

I.5. Antimony doped Tin Oxide (ATO)

Electrical properties can be improved with doping such as doping with antimony (Sb), cobalt (Co), iron (Fe), palladium (Pd), niobium (Nb), fluorine (F),indium (In); It has been achieved to improve tin oxide (SnO_2) properties. Antimony (Sb) on SnO_2 is one of the most studied dopants in the field among these dopants. Antimony-doped tin oxide (ATO), being an n-type, wide band gap semiconductor ($\geq$3.6 eV) with special properties (high transmittance in the visible range and high reflectance in the infrared, excellent electrical conductivity, greater carrier mobility and good mechanical stability), is used in different devices, like solar cells as transparent, protective electrodes, flat panel collectors as spectral selective windows, sensors for the detection of gases, sodium lamps and varistors [10].

Conclusion

In this chapter we have known the transparent conductive oxides which have the double characteristics of (Electrical conductivity and optical transmission), and from TCOs types we have specialized our study on Tin oxide in which we have proposed to study its The films are polycrystalline with tetragonal crystal structural, optical and electrical properties in order to ameliorate its characteristics.

Chapter II

Thin Film Deposition Methods

Thin Film Deposition Methods

The transparent conductive oxide (TCO) is obtained in the form of thin film by the deposition technique. The deposition ways of the thin layers are different from one another. It refers to the diversity of the domain where we use these layers. Scientifically, these ways are divided into two parts: physical and chemical such as Spray pyrolysis which is the spot of our study in this work.

II.1. Thin Film

Thin film technology is the basic of astounding development in solid state electronics. The usefulness of the optical properties of metal films, and scientific curiosity about the behavior of two dimensional solids has been responsible for the great interest in the study science and technology of the thin films. Thin film studies have directly or indirectly advanced many new areas of research in solid state physics and chemistry which are based on phenomena uniquely characteristic of the thickness, geometry, and structure of the film [43,44].

Thin films are especially appropriate for applications in microelectronics and integrated optics. However the physical properties of the films like electrical resistivity do not substantially differ from the properties of the bulk material. Thin film is defined as a low–dimensional material created by condensing, one– by –one, atomic/molecular/ionic species of matter. For a thin film the limit of thickness is considered between tenths of nanometer and several micrometers [44,45,46].

Some of the factors, as conditions preparation, which determine the physical, electrical, optical and other properties of a film rate of deposition, substrate temperature, environmental conditions, residual gas pressure in the system, purity of the material to be deposited, in homogeneity of the film, structural and compositional variations of the film in localized or wider areas etc [47,48].

II.2. Stages of Thin Films Growth

In order to obtain fine quality thin films for device applications and for better understanding the properties, the concepts regarding the nature of the films should be understood. The ideal condition of the film formation involves the deposition of the material atom by atom (or molecule by molecule) and layer by layer with proper time interval between the two successive depositions so that, they can occupy the minimum potential energy

configuration with respect to the substrate and subsequently on the previously deposited layers [49].

For more understanding thin films, the following properties illustrate various mechanisms occurring at different stages of film growth. There are several stages in the growth process, from the initial nucleation of the deposits to the final continuous three dimensional film formation states [479]:

II.2.1. Nucleation

The nucleation is the primary process for all deposition. The common process of addition, adsorption, desorption, migrations, etc. of atoms is called nucleation or small cluster formation which is schematically shown in (figure II-1-a).

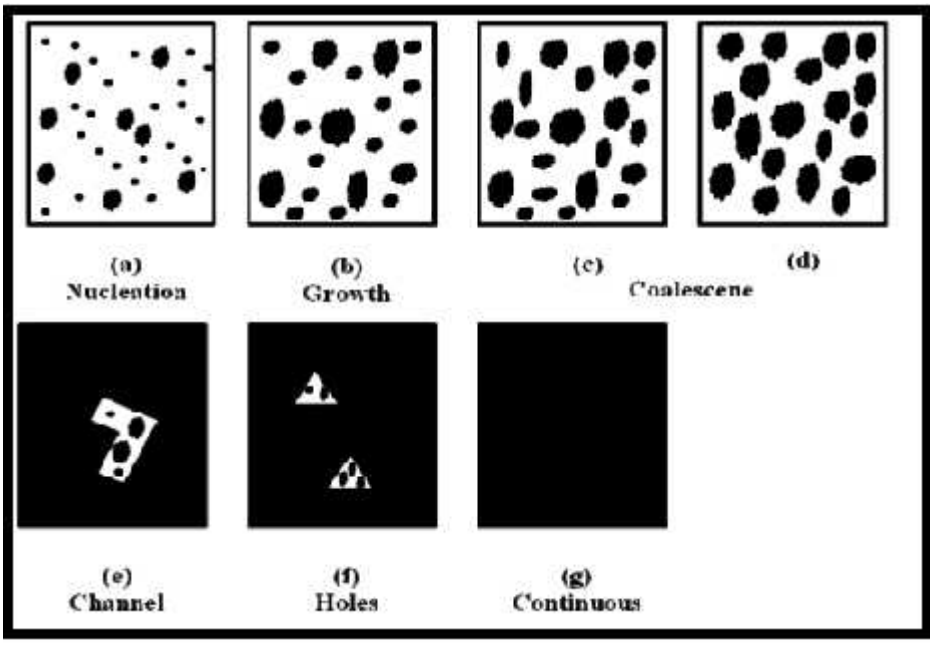

Figure (II-1): Schematic diagram showing stages of thin film growth [49].

II.2.2. Island structure

The islands consist of comparatively larger nuclei (>10 Å) and generally of three dimensional natures with their height, however, much less than their lateral dimensions. The formation of these islands and their growth take place either by direct addition of atoms from the vapor phase or from other environment or by the diffusion controlled process (see figure II-1-b). The diffusion controlled process is moreover commonly observed except at low substrate temperature.

II.2.3. Coalescence

As mentioned in the second stage, as islands grow they develop some characteristic shapes and then with further growth, coalesce with the neighboring ones by rounding off their edges near the joining region (neck) where these deposits assume a liquid like structure. The coalescence involves considerable transfer of mass between islands by diffusion. Small islands disappear rapidly. The process resembles the sintering of bulk powder where the individual particles assume spherical shapes due to the lowering of their surface energies. During coalescence of two islands which occurs at their necks recrystallisation as well as annealing takes place leading to some definite shapes of larger islands (figure II-1-c and d).

II.2.4. Channel and Holes

As the coalescence continues with deposition, there will be a resultant network of the film with channels in between (figure II-1-e). These channels do not remain void, but the secondary nuclei start to grow within these void spaces in the channel. Sometimes these channels may not be completely filled up even with increasing film thickness thus leaving some holes or gaps in the aggregate mass (see figure II-1-f). With increasing film thickness, these holes or gaps will decrease in size.

II.2.5. Continuous film

When these gaps are completely bridged by the secondary nuclei, films will be continuous. However, it often happens that some void space may still remain unbriged. In an ideal continuous film there should not be any gap in the aggregate mass. Such a stage in the film can be attained at certain average film thickness (figure II-1-g).

II. 3. Thin Film Deposition Processes

Thin film materials are the key elements of continued technological advances made in the fields of optoelectronic, photonic, and magnetic devices. The processing of materials into thin films allows easy integration into various types of devices. The properties of material significantly differ when analyzed in the form of thin films.

The vast varieties of thin film materials use in their deposition processing and fabrication techniques methods which are possible to be classified in two ways as following [50,51]: Physical Process and Chemical Process. The thin film deposition methods are summarized in figure (II-2).

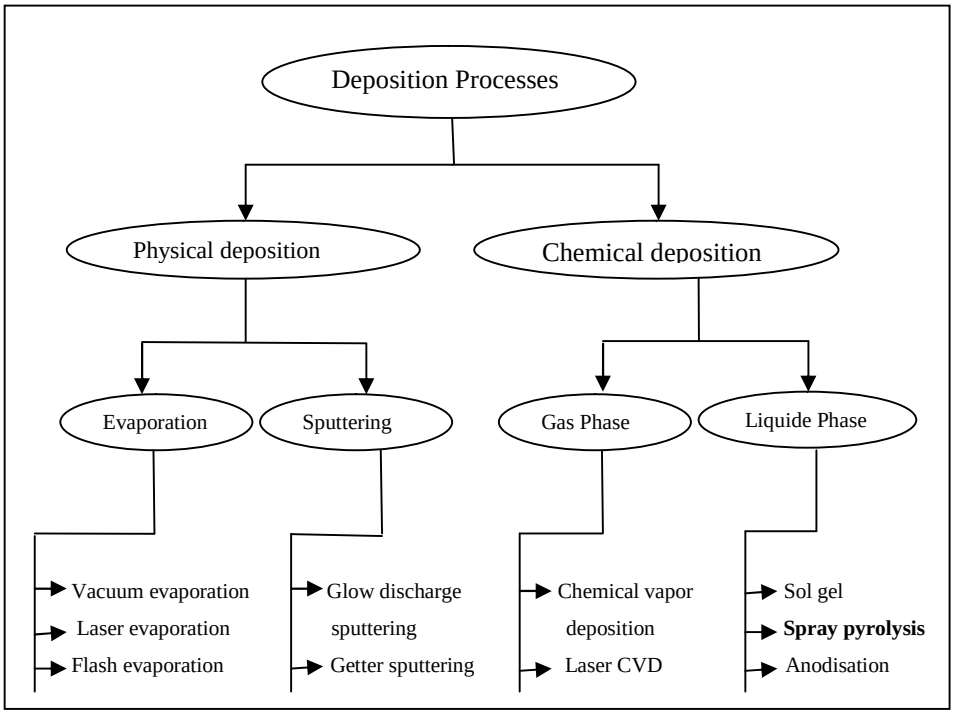

Figure (II-2): Classification of Thin Film Deposition Techniques [52].

II.3.1. Physical Processes

Physical method covers the deposition techniques which depends on the evaporation or ejection of the material from a source, i.e. evaporation or sputtering [53,54],

II.3.1.1. Evaporation

Evaporation is a physical vapor deposition (PVD) process in which the wafer (substrate) is placed in a chamber and subjected to very low pressures as the chamber are removed using a vacuum pump. One the chamber is free of residual gases, the material to be deposited is subjected to a temperature sufficient to cause it to evaporate. The evaporated molecules are dispersed throughout the chamber, landing on the wafer (and the chamber walls) and condensing, coating the wafer uniformly. Evaporation or sublimation techniques are widely used for the preparation of thin layers. A very large number of materials can be evaporated and, if the evaporation is undertaken in vacuum system, the evaporation temperature will be very considerably reduced, the amount of impurities in the growing layer will be minimized [55].

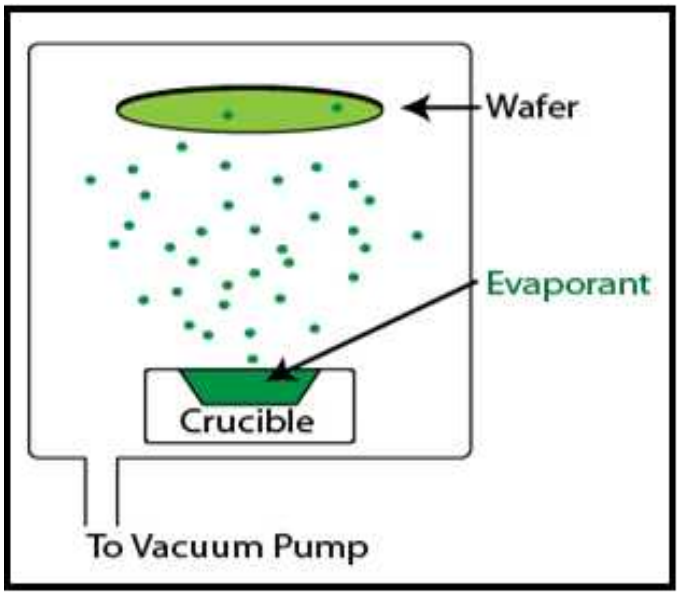

Figure (II-3): Schematic diagram of the evaporation technique [56].

II.3.1.2. Sputtering

Sputtering is another physical vapor deposition process occurs in a vacuum chamber. A large piece of the material to deposited, known as a target, is bombarded with high energy argon ions from a glow discharge. When the argon ions strike the target, they knock off target atoms and molecules, which are then conveyed through the vacuum to the wafer (i.e. substrate), where they condense and form a thin film. Sputtering is most commonly used for depositing metal films, but, like evaporation, can also deposit insulating films with some slight process and equipment variations [57].

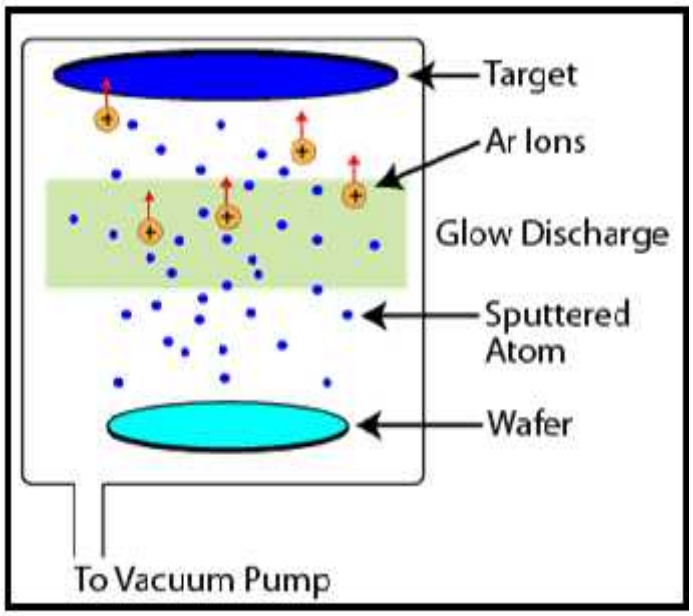

Figure (II-4): Schematic diagram of the sputtering technique [58].

Each method has his advantages and disadvantages as it recapitulated in table (II-1)**.**

Table (II-1): Advantages and Disadvantages of Physical process.

Deposition process	**Advantages**	**Disadvantages**
Evaporation [59]	- Highest purity (Good for Schottky contacts). - To low pressures.	- Poor step coverage, - Lower throughput due to low vacuum. - high cost.
Sputtering [60]	- Better step coverage. - Less radiation damage than evaporation. - Easier to deposit alloys.	- Some plasma damage including implanted argon; - Good for ohmics, not Schottky diodes; - The higher pressure produces better step coverage due to more random angled delivery; - high cost

II.3.2. Chemical Process

Chemical methods depend on physical properties. Structure-property relationships are the key features of such devices and basis of thin film technologies. Underlying the performance and economics of thin film components are the manufacturing techniques on a specific chemical reaction [61].

II.3.2.1. Chemical Vapor Deposition

Chemical vapor deposition can be defined as a material synthesis method in which the constituents of vapor phase react together to form a solid film at surface. The chemical reaction is an essential characteristic of this method; therefore, besides the control of the usual deposition process variables, the reactions of the reactants must be well understood. Various types of chemical reactions are used in CVD for the formation of solids are pyrolysis, reduction, oxidation, hydrolysis, synthetic chemical transport reaction etc, a numbers of forms of CVD in wide use and are frequently referenced in the literature [62].

a) Metal-organic CVD (MOCVD), CVD processes based on metal-organic precursors;
b) Photo-Enhanced Chemical Vapor Deposition (PECVD);

c) Laser-Induced Chemical Vapor Deposition (LCVD);

d) Low-pressure CVD (LPCVD), CVD processes at sub atmospheric pressures. Reduced pressures tend to reduce unwanted gas phase reactions and improve film uniformity across the wafer;

e) Plasma-enhanced CVD (PECVD), CVD processes that used plasma to enhance chemical reaction rates of the precursors. PECVD processing allows deposition at lower temperatures, which is often critical in the manufacture of semiconductors.

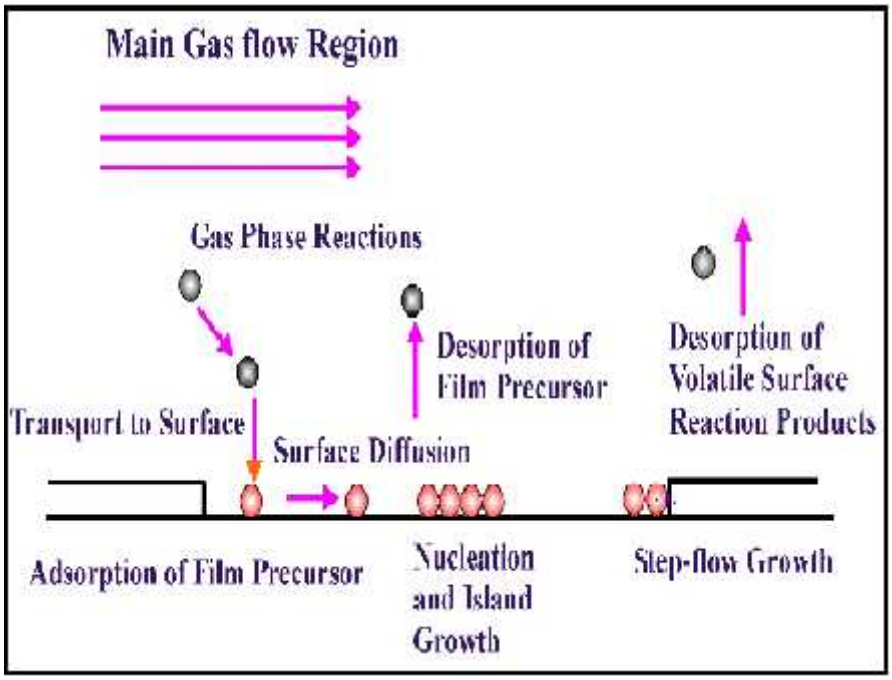

Figure (II-5): Deferent stages of chemical vapor deposition (CVD) process [63].

II.3.2.2. Sol-gel

Sol-Gel is a chemical method using for preparation of metal oxide-type materials such as ceramics and glasses. Initially, it consists of a stable suspension (Sol) of chemical precursors in solution. These "Sol" was transformed to a "Gel" during the gelling step result of chemical interactions between species in suspension and solvent, to give an expanded three-dimensional solid lattice through the liquid medium. The obtained gel is "wet" subsequently it was transformed into dry amorphous material by removal of solvents (to obtain an air-gel) or by evaporation under atmospheric pressure (to obtain xerogel) [64].

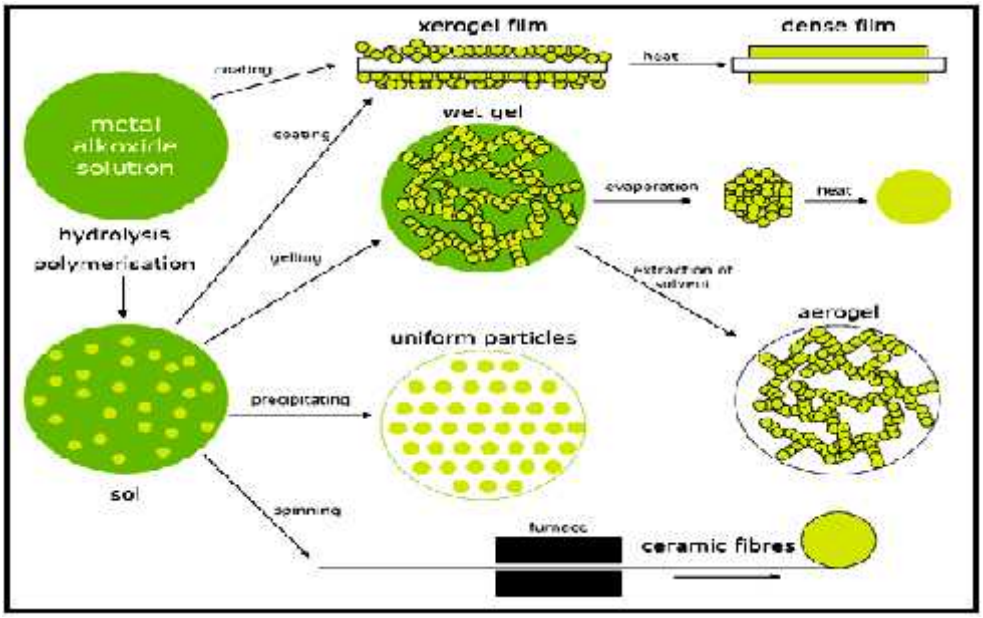

Figure (II-6): Sol-gel mechanism [65].

Table (II-2): Advantages and disadvantages of Chemical Process.

Deposition process	Advantages	Disadvantages
Chemical Vapor Deposition [66]	- The versatility of the CVD process. - Materials in excess 99.9% of theoretical density. - Economical in production, since many parts can be coated at the same time.	- CVD tends to increase the cost of fabrication. - Limitation can be overcome using single source chemical precursors. - The use of more sophisticated reactor and/or vacuum system by CVD variants.
Sol gel [67]	- Smaller particle size and morphological control in powder synthesis. - Sintering at low temperature also possible. - provides high purity homogeneous materials.	- High cost of the precursors. - Long process duration. - Difficulties in the synthesis of monoliths.

In all deposition process, atoms collect on the substrate in structures that initially have low density and low order compared to the equilibrium structure of the film material. The mechanisms by which crystallographic order is gradually recreated within the deposited film

have been subjects of intense study, as reviewed by Machlin and other investigators cited therein [II-7]. A key feature of these processes is the creation of stress in the newly deposited film.

II.4. Spray Pyrolysis

Different processes for the preparation of films have been employed, such as: physical vapor deposition (PVD), chemical vapor depositions (CVD), sol-gel and spray pyrolysis. However, Compared to the other techniques mentioned, spray pyrolysis requires simple and inexpensive equipment and has as main advantages the easy addition of doping materials, good reproducibility, high films growth rate, chemical homogeneity in the final product and the potential for deposition over large areas. The films, dense or porous, have thicknesses ranging from 0.1 to 10 µm [68].

Spray pyrolysis is a technique through which dense or porous films and powders can be obtained by controlling the deposition parameters. This technique involves the atomization of a precursor solution that is thrown directly over the heated substrate where the film will be formed [69].

II.4.1. Principle

Spray pyrolysis involves a thermally stimulated chemical reaction between constituent ions to form the required compound. In this technique, a solution containing the soluble salts of the constituent atoms of the required compound is sprayed on to a hot substrate in the form of fine droplets, using a sprayer. Usually compressed air will be the carrier gas. But compressed nitrogen is also used as carrier gas to avoid the presence of oxygen. The sprayed droplets reaching the hot substrate surface undergo pyrolytic decomposition and form the compound as a thin film on the surface of the hot substrate. In fact it is the hot substrate which provides the thermal energy needed for the decomposition and subsequent recombination of the constituent species. The other volatile by products and the excess solvents are converted into vapor phase and are removed from the site of chemical reaction by using an exhaust fan [70].

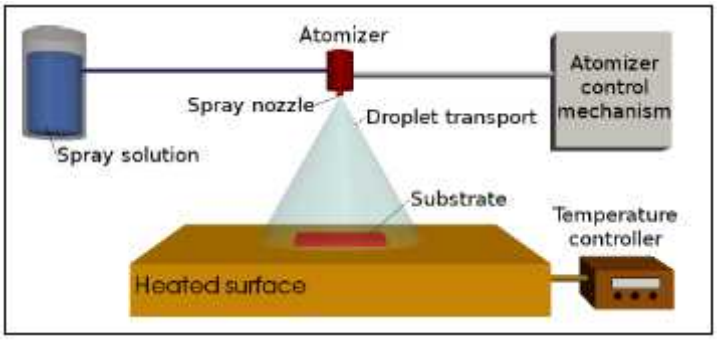

Figure (II-7): The schematic of the spray pyrolysis [71].

II.4.2. Chemical Aspects

The chemicals used for spray pyrolysis have to satisfy the following conditions:

1. On thermal decomposition, the chemicals in solution form must provide the species/complexes that will undergo a thermally activated chemical reaction to yield the desired thin film material;

2. The remaining constituents of the chemicals, including the carrier liquid should be volatile at the spray temperature. For a given thin film material, the above conditions can be met by a number of combinations of chemicals [70].

II.4.3. Characteristic features of the spray pyrolysis process

The growth rate of the sprayed films depends upon the chemical and topographical nature and temperature of the substrate, the chemical nature and concentration of spray solution and its additives. Another factor that affects the growth rate is the spray parameters like scanning speed of the spray head, the distance of the spray head from the substrate, the angle of incidence of the droplet on the substrate etc. The thickness of the film increases almost linearly with spraying time, i.e. with the amount of sprayed solution. In general, the spray pyrolysis process affects the substrate surface. When it is not desirable for the substrate to take part in the pyrolytic reactions, neutral substrates such as glass/quartz, ceramics are employed.

Compared with other techniques for obtaining films, this technique presents a simple experimental arrangement and is a cost effective method, mainly due to its simple equipment. It does not require the use of high quality reagents and substrates. The composition of the films can be easily controlled with the reagents used in the precursor solution. Several types of films have been deposited by spray pyrolysis, and this technique has been used for decades in various industries, such as in the production of glass, solar cells and electrical conductive electrodes [72].

II.4.4. Advantages and disadvantages of Spray Pyrolysis

Advantages [5]

- Low cost (inexpensive apparatus, does require high quality targets or vacuum);
- Easy control of composition and microstructure (facile way to dope material by merely adding doping element to the spray solution;
- Deposition at moderate temperatures of 100-500°C;
- Technological ability for mass production.

Disadvantages [5]

- Possible oxidation of sulfides when processed in air atmosphere;
- Difficulties with growth temperature determination;
- After long processing time spray nozzle may become cluttered;
- Films quality may depend on the droplet size and spray nozzle.

Conclusion

It has been shown in this chapter, even if it is briefly, the cognition of the thin film for the TCOs and its stages of growing. Also, we have mentioned some methods of deposition to get that film. We have proposed in each method its advantages and disadvantages where we focused on the chemical process: Spray pyrolysis, which is the base of our experimental study of elaborated SnO_2.

Chapter III

Characterizations Methods and Experimental

Characterizations Methods and Experimental

Characterizations methods of transparent conductive oxides thin films are different, there are a lot of structural, electrical and optical methods which specialize the thin films and help to obtain characteristics (band gap, absorption coefficient, grain size, thickness film types……) of the deposited thin films. In this chapter we will study some experimental methods to determine the characteristics of the transparent conductive oxide (SnO_2).

III.1 Thin films description techniques

In order determine structural, electrical, optical properties and thickness for thin films, we have used different method describe below:

III.1.1 Determination of optical properties

III.1.1.1 UV-visible spectroscopy

In conventional spectrometers electromagnetic radiation is passed through the sample which is held in a small square-section cell (usually 1 cm wide internally). Radiation across the whole of the ultraviolet/visible range is scanned over a period of approximately 90s, and radiation of the same frequency and intensity is simultaneously passed through a reference cell containing only the solvent (references). Photocells then detect the radiation transmitted and the spectrometer records the absorption by comparing the difference between the intensity of the radiation passing through the sample and the reference cells shows in Figure (III-1). In the latest spectrometers radiation across the whole range is monitored simultaneously [73].

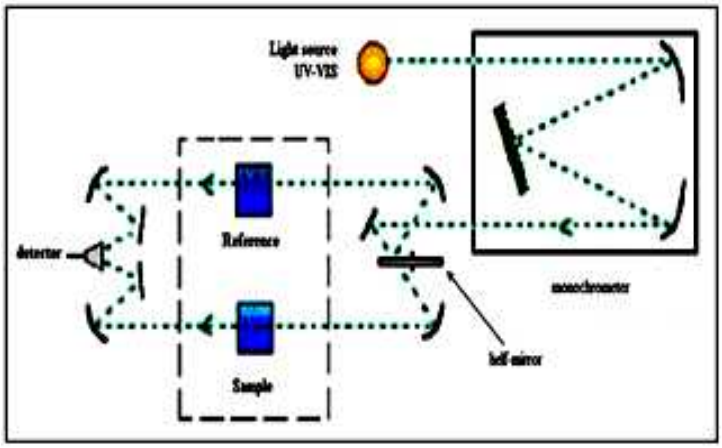

Figure (III-1): Diagram showing how the ultraviolet/visible spectrometer works [74].

No single lamp provides radiation across the whole of the range required, so two are used. A hydrogen or deuterium discharge lamp covers the ultraviolet range, and a tungsten filament (usually a tungsten/halogen lamp) covers the visible range. The radiation is separated according to its frequency/wavelength by a diffraction grating followed by a narrow slit. The slit ensures that the radiation is of a very narrow waveband, i.e. it is monochromatic. The cells (references slides glasses in the spectrometer must be made of pure silica for ultraviolet spectra because soda glass absorbs below 365 nm, and pyrex glass below 320 nm). Detection of the radiation passing through the sample or reference cell (slides glasses) can be achieved by either a photomultiplier or a photodiode. The spectrum is produced by comparing the currents generated by the sample and the reference beams. Modern instruments are self-calibrating, though the accuracy of the calibration can be checked if necessary. Wavelength checks are made by passing the sample beam through glass samples that have precise absorption peaks, and the absorption is calibrated by passing the sample beam through either a series of filters, each with a specific and known absorption, or a series of standard solutions [75,76].

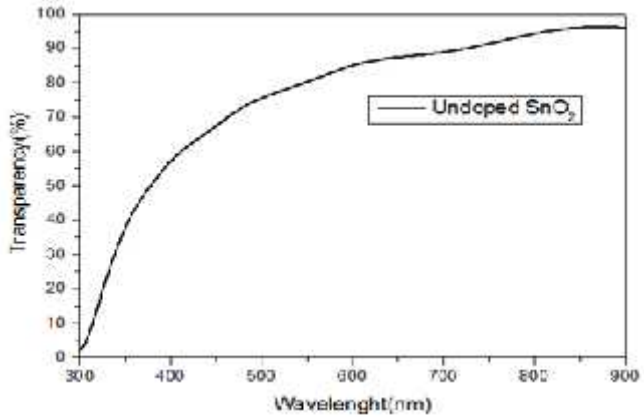

Figure (III-2): Ideal spectrum of transmittance of SnO_2 deposited by spray pyrolysis, from our work.

III.1.1.2 Absorption coefficient

Based on transmittance spectra, we can determine the absorption (***a***) and extinction (***k***) coefficients for the materials formed, we use the relation, which known by the beer-lambert low [77].

$$T = \exp(-\alpha . d) \qquad (\mathrm{III}-1)$$

Comparing the relation (III- 1) with the formula (I-8), we find that the coefficient $((1-R) \approx 1)$, this is due to negligence of the interaction of light on the faces (reflection): air and film, air and substrate, film and substrate.

Insertion the logarithm (ln) to the formula (III-1), we find a absorption coefficient (α) as follows: $lnT = -\alpha.d$, So $\alpha = \frac{1}{d} ln \frac{1}{T}$, but on the transmittance spectra by (T%) so:

$$\alpha = \frac{1}{d} \ln \frac{1}{T\%} \qquad (\text{III} - 2)$$

Based on a formula (III-2), we can determine absorption coefficient, also the extinction coefficient *k.*

III.1.1.3 Band gap

The band gap energy is calculated from the Tauc plot, versus the photon energy $h\nu$ [78].

$$(\alpha h\nu)^2 = A(h\nu - E_g) \qquad (\text{III} - 3)$$

where A: constant.

If $(\alpha h\nu)^2$ is extrapolated to the x-axis intersection ($(\alpha h\nu)^2$=0), formula (III-3) implies that the photon energy equals the band gap energy ($h\nu \approx Eg$). This method is commonplace to extract band gap energies from transmission data. The figure follow shows a plot for SnO_2 film non-doping.

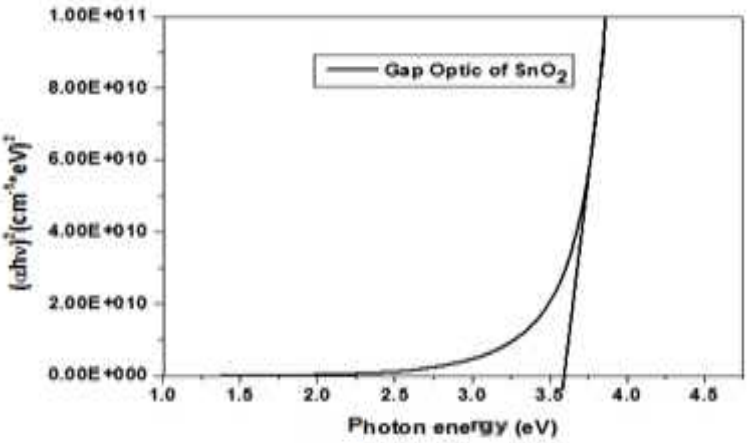

Figure (III-3): the variation plot $(\alpha h\nu)^2$ function $h\nu$ for SnO_2 film, from our work.

III.1.1.4 Urbach energy

Urbach energy defined as the width of the localized states available in the optical band gap that affects the optical band gap structure and optical transitions. The Urbach tail is determined by the following relation (Urbach 1953) [79,80]:

$$\alpha = \alpha_0 \exp\left(\frac{E}{E_u}\right) \qquad (\text{III} - 4)$$

Where E: The photon energy (i.e. $h\nu$);

α_0: Constant;

E_u: Urbach energy, which refers to the width of the exponential. It is possible to determine the value of urbach energy E_u, through drawing a statement $\ln \alpha$ as function of $h\nu$:

$$ln\,\alpha = ln\alpha_0 + \frac{h\nu}{E_u} \qquad (\text{III} - 5)$$

This is by calculating the slope of the plot $\frac{1}{E_u}$ output.

III.1.2 Determination of electrical properties

In order to determine of the electrical properties, we uses the 4-probe method, which determining the sheet resistance based on electrical resistivity.

Four probe method

The 4-point probe set up figure (III-4) consists of four equally spaced tungsten metal tips with finite radius. Each tip is supported by springs on the end to minimize sample damage during probing. The four metal tips are part of an auto-mechanical stage which travels up and down during measurements. A high impedance current source is used to supply current through the outer tow probes; a voltmeter measures the voltage across the inner two probes, to determine the sample resistivity. Typical probe spacing is ~ 1 mm [81].

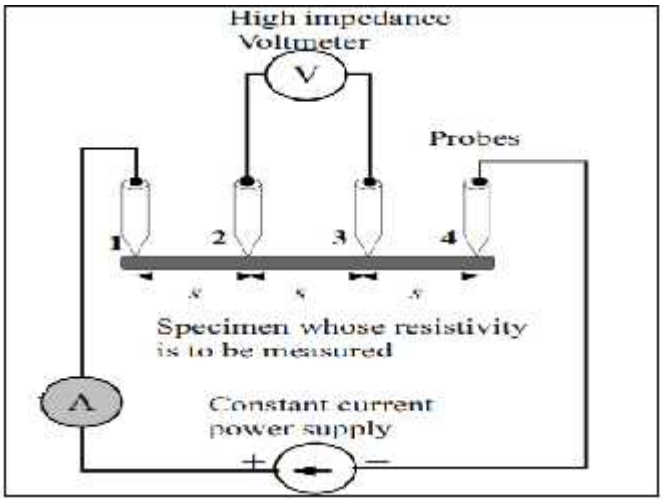

Figure (III-4): Four probe method of measuring resistivity of a specimen [81].

In figure (III-4) for the Four probe method, s is spacing between point probes, it unit by meter (m).

The two outer probes are used for sourcing current and the two inner probes are used for measuring the resulting voltage drop across the surface of the sample. The volume resistivity is calculated as follows [10,82]:

$$\rho = \frac{\pi}{\ln 2} \cdot \frac{V}{I} \cdot d \qquad (III-6)$$

where ρ: the volume resistivity ($\Omega.cm$);

V: the measured voltage (volts);

I: the source current (amperes);

d: the sample thickness (cm);

Based on a formula (I-2), we deduce the following:

$$R_s = \frac{\pi}{\ln 2} \cdot \frac{V}{I} = 4.53 \frac{V}{I} \qquad (III-7)$$

III.1.3 Determination of structural properties

We will use X-Ray diffractometer for determining the thin films structural properties, i.e. determining the lattice parameters, and grain size.

X-Ray Diffraction (XRD)

XRD is a precise and popular method for determining the crystal Structures of thin films and it is essentially non-destructive. It gives information about the crystal structure, orientations, lattice constants, crystallite size and composition with the help Joint Committee Power Diffraction Standards (JCPDS) of the sample. Analysis of the diffraction pattern obtained, by comparing with the JCPDS data can reveal the existence of different crystallographic phases in the film, their relative abundance and preferred orientations. From the width of the diffraction line the average grain size of the film can also be estimated [83].

Much of our knowledge about crystal structure and the structure of molecules as complex as DNA in crystalline form comes from the use of x-rays in x-ray diffraction studies. A basic instrument for such study is the Bragg spectrometer [46]. For thin films, the powder technique in conjunction with diffractometer is most commonly used. In this technique the diffracted radiation is detected by the counter tube, which moves along the angular range of reflections.

The intensities are recorded on a computer system. Figure (III-5) shows the schematics of X-ray diffractometer.

Diffraction in general occurs only when the wavelength of the wave motion is of the same order of magnitude as the repeat distance between scattering centers. This condition of diffraction is nothing but Bragg's law and is given by [84,85]:

$$2d_{hkl}\sin\theta = n\lambda \qquad (\text{III}-8)$$

where d_{hkl}: inter-planer spacing;

θ: The Bragg angle;

n: The order of the spectrum;

λ: The wavelength of X-rays.

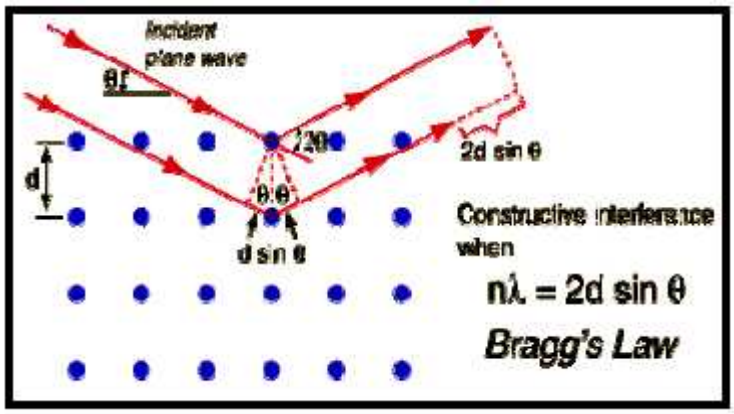

Figure (III-5): schematic of X-rays Diffraction [86].

Using the *d* values the set of lattice planes (***hkl***) are identified from the standard data and the lattice parameters are calculated using the following relations. For tetragonal system, such as SnO_2 [87]:

$$\frac{1}{{d_{hkl}}^2} = \frac{h^2+k^2}{a^2} + \frac{l^2}{c^2} \qquad (\text{III}-9)$$

where a and c: the lattice parameters

The sample used may be powder, single crystal or thin film. The crystallite size of the deposits is estimated from the full width at half maximum (FWHM) of the most intense diffraction line by Scherrer's formula as follows [88]:

$$D = \frac{0.9\lambda}{\beta\cos\theta} \qquad (\text{III}-10)$$

where D: The crystallite size;

β: The full width at half maxima of the peak (FWHM) in radians.

This technique is not useful for identification of individuals of multilayers or percentage of doping material.

III.1.4 thin film thickness Measuring

We will use a program named Hebal optics for deducing the thickness of the films.

III.2 Experimental installation

III.2.1. Spray Apparatus

The experimental setup used in the laboratory (VTRS) for the preparation of undoped and Sb doped SnO_2 thin films is shows in figure (III-6).

Figure (III-6): Photo for Spray pyrolysis Apparatus.

Names of the numbered elements are illustrated in table (III-1).

Table (III-1): represented Spray pyrolysis home made.

Number	System components
1	Solution reservoir and Atomizer
2	Air compressor
3	Nozzle
4	Substrate holder
5	Temperature controller
6	Moving nozzle

III.2.2. Preparation of spray solution

SnO_2 solution was prepared by dissolving 0.5 M Tin chloride ($SnCl_2$, $2H_2O$) in mixture doubly distilled water and methanol under volume ration (1:1). methanol solution (99.995%) of absolute purity is provided from Sigma Aldrich; Few drops of acetic acid were added to the solution. The mixed solution was stirred at 60°C for 120 min to yield a clear and transparent solution. The doped solution was prepared by adding to the precedent solution ($SbCl_3$, $7H_2O$) as doping source. The weight percentages of (Sb/Sn) were in 0 - 1 wt. % average. The solution became clear and homogeneous after stirring for 60 min at 50 to 70°C. The substrate was microscope glass having (ref R217102) and size of (7.5 cm x 2.5 cm x 0.13 cm); prior to deposit, the substrate was cleaned with alcohol in an ultra sonic bath and blow-dried with dry nitrogen gas. Undoped and Antimony doped tin oxide (SnO_2 and SnO_2:Sb) thin films were prepared using a chemical spray pyrolysis technique as described elsewhere. Stannous chloride ($SnCl_2$ $2H_2O$) was used as a precursor for tin. This tin precursor dissolved in double distilled water and methanol (volume ratio 1:1) with adding few drops of (HCl). The precursor concentration was (0.1 M), served as a starting solution.

For Antimony doping, Antimony chloride ($SbCl_3$) was dissolved in doubly distilled water and added, with an appropriate amounts to achieve Sb concentration, to the starting solution. The Sb concentration in the stock solution was varied as 0, 0.6, 0.8, and 1 wt.% of course by adding appropriate amount of ($SbCl_3$). An R217102 microscopic glass slide in a size of ($75 \times 25 \times 1.1$ mm^3) was used as substrates which were cleaned with alcohol in a pyrolysis bath and distilled water, then blow-dried with dry nitrogen gas. A chromel–alumel and K type thermocouple were used for reading and controlling the optimized substrate temperature to 480 °C [10,89]. The resulting solutions were spray pyrolysis on the heated glass substrates under

uniform and fine droplets of 40 lm average diameter (given by the manufacturer). The time deposition was 3 min for each experiment. The sprayed solution on the heated substrate leads, at nuked eye, to uniform and homogenous ATO films. After deposition, the films were allowed to cool down naturally to room temperature (rt).

III.2.3. Preparation of SnO_2 Thin films

Tin oxide thin films were deposited on heated substrate at 475°C using homemade spray pyrolysis technique; a nebulizer was used as atomizer to produce uniform size droplets (diameter of droplet 5µm provided by manufacture); the droplets are undergone, via a nozzle, on the heated substrate. The nozzle performed an oscillating movement at constant velocity to scan the whole area of the substrate.

III.2.4. Characterization

For optical transmission spectra we have used an UV-visible spectrophotometer (Shimadzu, Model 1800) as shown in figure (III-7) spectral region 200-900 nm. The film thickness was estimated from the exhibited interference patterns of the transmission spectra.

Figure (III-7): Photo for uv-vis apparatus (Shimadzu, Model 1800).

Structural characterizations are carried out using a X-ray diffractometer (BRUKER - AXS type D8) equipped with X'Pert High Score under Cu K_α (λ=1.54056Å) radiation whereas the scanning range of (2θ) was between 20° and 80°. The grain size of the films was estimated using X'Pert High Score. The measurements were carried out at room temperature (rt).

Figure (III-8): Photo for X-Rays Diffraction apparatus (Brukers Advance D8 - type).

Conclusion

In this chapter we realized that it is possible to determine the electrical, optical and structural characteristics of thin films oxide layer doped and non-doped through the experimental results that we have done in comparison with the theoretical equations where we have known the components of the experimental machine and how to get thin films.

Chapter IV

Results and Discussion

Results and Discussion

We aim in this chapter to give principle characteristics of the elaborated thin films and the effect of dopant concentration of thin film such as structural properties by **X-ray** diffraction studies, optical and electrical properties by spectra transmittance and four probe respectively. Also, we will determine the films quality which we have prepared by spray pyrolysis method.

IV.1. Structural properties

IV.1.1. X-ray diffraction studies

XRD patterns of undoped and Sb doped SnO_2 with various amounts of Sb concentration (0–1 wt%) are shown in figure (IV-1). The analysis of those patterns revealed that the undoped and Sb doped SnO_2 films are polycrystalline tetragonal rutile phase of tin oxide (JCPDS card No. 041-1445) which belongs to the space group P42/mnm (number 136). It is perceptible from the XRD patterns of figure (IV-1), as it seen, that both the undoped and Sb doped tin oxide films grow along the preferred orientation of (211). The presence of other orientations such as (110), (101), (200), (310), and (301) also has been detected with considerable intensities for both undoped and doped tin oxide films.

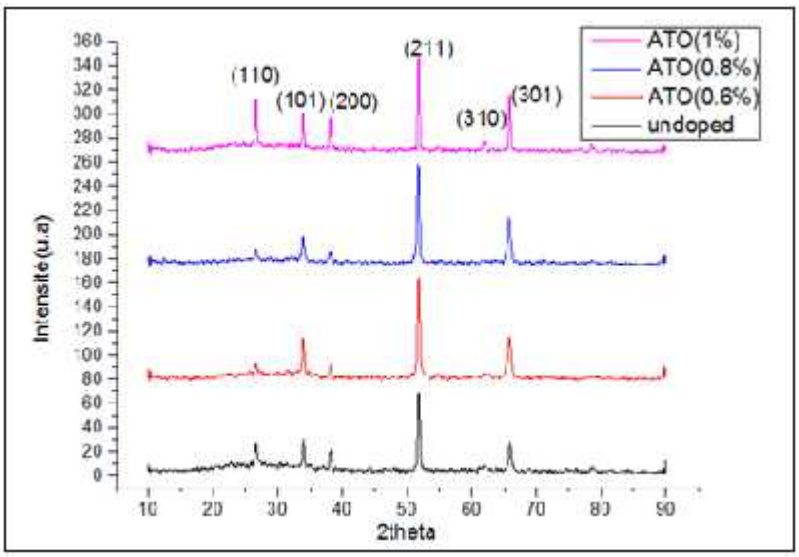

Figure (IV-1): XRD patterns of Sb (0–1 wt.%) doped SnO_2 thin films pyrolysisally sprayed.

A focused analysis, on (211) peaks, reveal that the later is located at about (51.82°) for the undoped SnO_2 whereas the values for the Sb doped ones, until 0.8 wt.% level, are lower than the undoped SnO_2 spectra, indicating that the inter-planar spacing of SnO_2 (211) increases after Sb doping which may due to that some Sb in Sb^{+3} states are incorporated into the SnO_2 lattice by

substituting for Sn^{+4} sites. With increasing Sb doping to 1 wt.%, the location of peak (211) return back toward the higher degree direction as it can be seen in figure (IV-1). This result implies that some Sb^{+3}, occupying the Sn^{+4} sites [10], miss its role in substituting for Sn and enter the interstitial sites, so the inter-planar spacing of SnO_2 (211) decreases to reach the value of inter-planar spacing of undoped SnO_2 one. The full width at half maximum (FWHM) of (211) peak decreases slightly, with increasing Sb concentration to 1 wt.%, indicating that the crystalline quality becomes better.

IV.1.2. Lattice parameters (a and c)

According to JCPDS data the standard lattice parameters of SnO_2 are a = b = 4.737 Å and c = 3.185 Å [89], and revealing slight decrease whereas the calculated ones of Sb doped SnO_2 films from XRD patterns data, according to the given equations [90]:

$$\frac{1}{d_{hkl}^{\,2}} = \frac{h^2 + k^2}{a^2} + \frac{l^2}{c^2} \qquad (IV-1)$$

and

$$2d_{hkl} \sin\theta = n\lambda \qquad (IV-2)$$

The values lattice parameters (a = b, and c) of undoped SnO_2 thin film are shown in Table (IV-2), where λ is the X-ray wavelength (1.5406 Å for CuKα1) and θ is the Bragg's angle, d_{hkl} is inter-planer spacing.

Table (IV. 1): shows the inter-planer spacing d_{hkl} and lattice parameters a, c of the undoped and Sb doped SnO_2 thin films between (0 −1 wt.%) at (211) peaks.

Sb (wt.%)	d_{hkl} (nm)	Lattice parameters	
		a (Å)	c (Å)
0	1.76332	4.715822	3.183337
0.6	1.764458	4.716154	3.189849
0.8	1.766504	4.735564	3.196527
1	1.76448	4.7285	3.190782

The lattice parameters (a and c) are found to increase with Sb doping concentration until 0.8 wt.%. This may be attributed to the substitution of Sn^{+4} ions by Sb^{+3} ones in the crystal lattice as their ionic radius match (ionic radius of Sn^{+4} = 0.74 Å and that of Sb^{+3} = 0.93 Å) [10] thin films pyrolysisally sprayed. In the same doping average (0 – 0.8 wt.% Sb). Beyond 0.8 wt.% to 1 wt.% the lattice parameters (a and c) then decrease, as shown in Table (IV-2), to reach its initials values.

IV.1.3. crystallite size

The average crystallite size deduced from the full width at half the maximum (FWHM) of (211) and planes was estimated using Scherrer's relation [91]:

$$D = \frac{0.9\lambda}{\beta \cos\theta} \qquad (IV-3)$$

where β is the observed angular width at half maximum intensity (FWHM) of the peak, The variation values of the grain size undoped and Sb doped SnO_2 thin films is shown in Table (IV-2).

Table (IV-2): shows the crystalline size *D* of the undoped and Sb doped SnO_2 thin films between (0 −1 wt.%).

Sb (wt.%)	ne size D eta)	ne (°2Th)	*D* (nm)
0	51.82	0.3247	33.253
0.6	51.76	0.3838	27.206
0.8	51.73	0.4133	24.933
1	51.79	0.3247	33.249

The grain size can be seen that the films are polycrystalline. With the increase of Sb concentration, the grains become more compact and gets little until 0.8 wt.% Sb doping, further the more the grain size gets bigger, so the degree of crystallization gets better as it was reported in the literature [89,90], which is consistent with the results of the XRD measurement.

IV.2. Optical properties

IV.2.1. Effect of the concentration of dopant on the spectra transmittance

The optical transmission T curves as a function of wavelength in 200 - 900 nm range of undoped and Sb doped SnO_2 thin films are shown in figure (IV-2). It is observed that the average transparency in the visible range is around ~85%. All films exhibit significant oscillations in the visible range; those oscillations, which are related to the interference phenomenon, are generated by the film thickness [10].

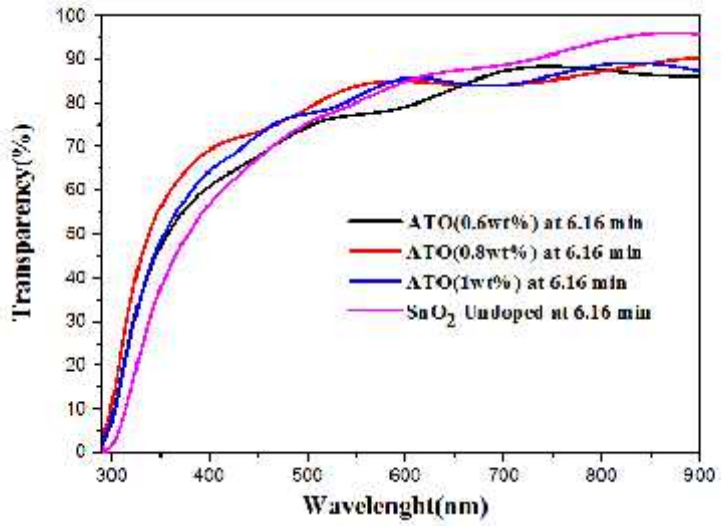

Figure (IV-2): Spectral transmittance plot of Sb (0 – 1 wt.%) doped SnO_2 thin films pyrolysisally sprayed.

The optically estimated film thickness is ranged between (700–935 nm) for the same given time deposition (6.16 min) as it is shown in table (IV-5). Also one can see that the decreased in transmission envelope region (around Eg region), T curves exhibits a shift toward lower wavelength for the Sb doping level lower than 0.8 wt.% with minimum value of transmittance, for wavelength more than 400nm, at this given doping level and then become large for 1 wt.% Sb doping level restoring its initials transmittance values. In heavily doped semiconductors, (having carrier concentration between 10^{19} and 10^{21} cm^{-3}), which is the case of 0.8 wt.% doped film.

IV.2.2. band gap

The optical gap (E_g) of the films can be obtained by plotting ($(\alpha h\nu)^2$ vs $h\nu$) ($\alpha$is the absorption coefficient and $h\nu$ is the photon energy) and extrapolating the straight-line portion of this plot to the energy axis as it was shown in figure (IV-3).

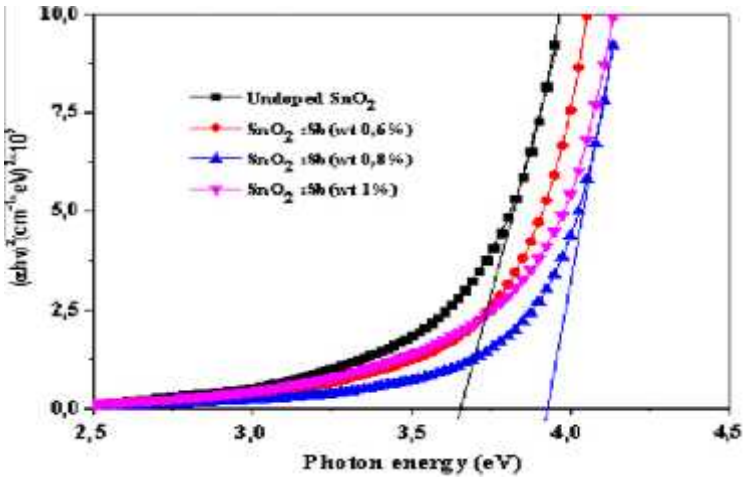

Figure (IV-3): Optical band-gap estimation, from Tauc relation, of Sb (0–1 wt.%) doped SnO_2 films pyrolysisally sprayed.

The obtained values of (E_g) for the undoped and Sb doped SnO_2 films are recapitulated in Table (IV-3). With increasing Sb concentration.

Table (IV-3): The optical gap (E_g) of Sb (0–1 wt.%) doped SnO_2 films pyrolysisally sprayed.

Sb (wt.%)	E_g (eV
0	3.651
0.6	3.829
0.8	3.929
1	3.869

From 0 to 0.8 wt.%, the absorption edge of the films shifts to shorter wavelength. The direct optical band gap (E_g) has increased from 3.651 to 3.929 eV. As Sb concentration increases further, the absorption edge shifts slightly to the longer wavelength and (E_g) has decreased from 3.929 eV to 3.869 eV. It was found that the E_g value for all the samples is over than that of the E_g value for pure SnO_2 (3.65 eV). This might be due to lower defect concentration in the crystals of Sb doped SnO2 due to Burstein-Moss band-filling effect, which causes the energy band widen (blue-shift) since Urbach energy (as will be seen bellow) remains practically constant with increasing the band gap indicating the independence of band gap on defects.

IV.2.3. Urbach energy

We can determine the value of urbach energy E_u, through drawing a statement $ln\,\alpha$ as function of photon energy $h\nu$, the plotting ($ln\,\alpha$ vs $h\nu$) of Sb (0 wt.%) doped SnO_2 films pyrolysisally sprayed is shown in figure (IV-4).

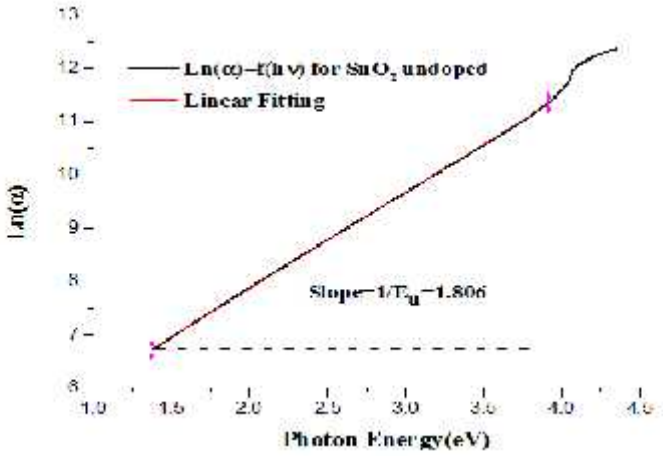

Figure (IV-4): shows the Urbach energy for undoped SnO_2thin films.

It was found that the Urbach energy remains practically constant with increasing the band gap indicating the independence of band gap on defects.

It is worth noting that a minimum of Urbach energy was reached with 0wt. % Sb doping SnO_2 thin films and remains constant as shown in table (IV-4), which means that the doping has less disorder in the film network. Such less disorder reveal the good crystalline of the thin films as it was correlated to the results carried out by DRX investigations in the above section

Table (IV-4): The Urbach energy of Sb (0–1 wt.%) doped SnO_2 thin films.

Sb (wt.%)	E_u (meV)
0	553
0.6	724
0.8	688
1	617

VI. 2.4. Determining the thickness of undoped and Sb doped SnO_2 thin films

We used the program Hebal Optics on computer to calculate thickness of undoped and Sb doped SnO_2 thin films. The results of calculating are shown in the table (IV-5).

Table (IV- 5): Thickness of Sb (0–1 wt.%) doped SnO_2 films pyrolysisally sprayed.

Sb (wt.%)	Thickness (nm)
0	806
0.6	935
0.8	700
1	700

IV.3. Electrical properties

The resistance sheet Rs as a function of Sb concentration. All Sb doped SnO_2 thin films were conducting at 300 K with resistivity values much less than of undoped SnO_2 one as it was shown in table (IV-6).

Table (IV-6): The resistance sheet *Rs* of Sb (0–1 wt.%) doped SnO_2 films.

Sb (wt.%)	*Rs* (Ω)
0	806
0.6	47.43
0.8	31.07
1	56.09

The resistance sheet *Rs* of the undoped SnO_2 is relatively high compared to the doped ones. For the 0 –1 wt.% doped films, the resistance sheet decreases at first from 138 to 31.07 **Ω** until 0.8 wt.% Sb doping level and then increases to reach 56.09 ($\mathbf{\Omega.cm^{-2}}$) for the 1 wt.% Sb doping level. Antimony can play two roles due to its two oxidation states namely Sb^{3+} (0.93) and Sb^{5+} (0.62). At doping level lower than or equal to 0.8 wt.%; substitutions of Sn by Sb resulting in increasing in the lattice parameters of SnO_2 which may considered as the predominate phenomenon. Doping level with Sb until 0.8wt.% create more oxygen vacancies than participating in free electrons increase, leading to decrease in the resistance sheet. Beyond 0.8wt

Sb doping, substitutions become less yielding to low oxygen vacancies which means low free electrons in band conduction B_c and high Rs.

Conclusion

Through this chapter we have known the suitable experimental conditions to prepare a un-doped SnO_2 film, and another one doped by antimony with different concentration.. Undoped and Sb doped SnO_2 thin films are successfully prepared using inexpensive spray pyrolysis technique (home made). Analysis, on (211) peaks, indicated that the inter-planar spacing of SnO_2 (211) increases, after Sb doping until 0.8 wt.% level, which may due to the substitution of some Sn by Sb into the SnO_2 network causing more oxygen vacancies generation free electron. With increasing Sb doping to 1%, it was revealed that Sb, occupying the Sn sites, miss its role in substituting for Sn and enter the interstitial sites leading to a feeble oxygen vacancies. The lattice parameters (a and c) are found to increase with Sb doping concentration until 0.8 wt.% level and then decrease.. The optical gap Eg has increased from 3.65 eV for undoped SnO_2 film to 3.92 eV at 0.8 wt.% Sb doping and then decreases. The average transparency in the visible range was found around 85%. The minimum resistance sheet (Rs) and maximum carrier concentration. We have reach to know that doping the tin oxide by antimony changes its characteristic.

General Conclusion

General Conclusion

In this work both theoretically and experimentally are exposed. We studied the (SnO_2) tin oxide because it is very available in the laboratory of El-oued university. So, we understood that this oxide is one of the n-type semiconductors. Some concepts and results were reached. In the first chapter we knew that the transparent conductive oxides are degenerate semiconductors: they contain high band gap ($\geq$ 3,1 eV). Thus it contains a high band gap between (3.6 – 4.2 eV). Despite this high band gap it is an electricity conductor and optically transparent at the sometime. In the second chapter we have exposed different deposition methods to get good thin films aving double properties (conductivity and transparent), we had chose one of those methods which is spray pyrolysis to prepare the films because of the availability of the experimental installation in the laboratory. This technique characterized by its advantages compared with other techniques because of the low cost, easiest and it can be done in the natural atmospheric pressure. In the third chapter we clarified the different methods to define and characterize the prepared films using such as X-RD and UV-visible and four probe technique. In the fourth chapter results occurred through some technique will be discussed and the analyzed.

All tin oxide films were prepared at the degree of 480^0C, which is suitable for the precipitation on the substrate surface, as we studied the properties of those different films for the undoped and (0-1%) antimony doped tin oxides. We have get the following results:

Undoped and Sb doped SnO_2 thin films are successfully prepared using inexpensive spray pyrolysis technique (home made). Analysis, on (211) peaks as preferred orientation, indicated that the inter-planar spacing of SnO_2 (211) increases, after Sb doping until 0.8 wt.% level, which may due to the substitution of some Sn by Sb into the SnO_2 network causing more oxygen vacancies generation free electron. With increasing Sb doping to 1%, it was revealed that Sb, occupying the Sn sites, miss its role in substituting for Sn and enter the interstitial sites leading to a feeble oxygen vacancies. The lattice parameters (a and c) are found to increase with Sb doping concentration until 0.8 wt.% level and then decrease.. The optical gap Eg has increased from 3.65 eV for undoped SnO_2 film to 3.92 eV at 0.8 wt.% Sb doping and then decreases. The average transparency in the visible range was found around 85%. The minimum resistance sheet (Rs) and maximum carrier concentration. We have reach to know that doping the tin oxide by antimony changes its characteristics. Highly antimony doped tin oxides will a subject for future studies with proposed method.

Reference

Reference

[1] **Afzal. Khan**, "Synthèse de Cuprates de Strontium ($SrCu_2O$) par MOCVD comme couche mince d'oxyde transparent conducteur de type P", Thése Pour obtenir le grade de Docteur de L'unversite de grenoble, (7 août 2006).

[2] **H. Bach and D. Krause.** "Thin Films on Glass. Springer-Verlag", Berlin, (2003).

[3] **Zhigang R. Li and Hong Meng**, "Organic Light-emitting Materials and Devices". CRC Press, USA, (2007).

[4] **B. O'Neill,** "Indium: Supply, Demand and Flat Panel Displays, Presented at Minor Metals", London, (June 2004).

[5] **Dedova. Tatjana. PhD**, "Chemical spray pyrolysis deposition of Zinc sulfide Thin Film and Zinc Oxide Nanostructured Layers", Volume 20, (2009).

[6] **K. Baedeker**, Ann. Phys, 22:749–766, (1907).

[7] **G. Rupprecht,** Z. Phys (1954), 139, 504.

[8] **B. Benhaoua, S. Abbas, A. Rahal, A. Benhaoua, M.S. Aida,** "Effect of film thickness on the structural, optical and electrical properties of SnO: F thin films prepared by spray ultrasonic for solar cells applications", Superlattices and Microstructures 83 (2015) 78–88.

[9] **K. L. Menouer**, "Etude et réalisat ion d'une cellule solaire multicouches du type Si-SiO_2-SnO_2-ZnO par APCVD", thèse de doctorat, Université Mouloud Mammeri de TIZIOUZOU,(2011).

[10] **A. Rahal, A. Benhaoua, Ch. Bouzidi, B. Benhaoua, B. Gasmi,** "Effect of antimony doping on the structural, optical and electrical properties of SnO_2 thin films prepared by spray ultrasonic", Superlattices and Microstructures 76 (2014)105–114.

[11] **J. Nishino and Y. Nosaka,** "Low température preparation of ZnO by a nearby vaporizing chemical vapor deposition method", Journal of Crystal Growth, Vol.268, (2004).

[12] **Clark I. Bright,** Review of Transparent Conductive Oxides (TCO), Society of Vacuum Coaters, (2007).

[13] **D.E. Carlson, C.R. Wronski,** "Amorphous Silicon", Topics in Applied Physics **Vol. 36**, 287-329, (1979).

[14] **M. Hiramatsu, K. Imaeda, NHorio and M. Nawata,** Journal of Vacuum Science and Technology A **16**, 669, (1998).

[4] **B. O'Neill,** "Indium: Supply, Demand and Flat Panel Displays, Presented at Minor Metals", London, (June 2004).

[15] **M. Oh, I. Seo**, "Enhanced performance of GaN-based green light-emitting diodes With gallium-doped ZnO transparent conducting oxide", J. Electron. Mater. 43 (2014) 1232–1236.

[16] **P.Y. Liu, J.F. Chen, W.D. Sun**, "Vacuum", 76 (2004) 7–11.

[17] **D. Lambe Y.Y. Proskuryakov, K. Durose, J. Major, M. Al Turkestani, V. Barrioz**, "Thin solid films", 518 (2009) 1222-1224.

[18] **G. Gordon**, "MRS Bulletin", 25(2000) 52-57.

[19] **B.G. Lewis and D.C**, Paine. MRS Bull, 25 No.8:22–27, (2000).

[20] **H. Sato and al,** "Thin Solid Films", 236:27–31, (1993).

[21] **H. Demiryont**, SPIE Newsroom DOI: 10.1117/2.1200608.0340, (2007).

[22] **K.S. Ramaiah, V.S. Raja,** "Structural and electrical properties of fluorine doped tin oxide films prepared by spray- pyrolysis technique", Applied Surface Science, Vol. 253, (2006).

[23] **H. Kawazoe and al**, "Oxide thin film", US Patent (US 6294274 B1), Sep. 25, (2001).

[24] **M. Chen, Z.L. Pei, X. Wang, C. Sun and L.S. Wen**, Phys. D: Appl. Phys. **33**, 2538 (2000).

[25] **J.M. Dekkers**, "Transparent Conducting Oxides on polymeric substrates by pulsed laser deposition", Ph.D. thesis University of Twente, Enschede, The Netherlands, geboren op 8 Augustus (1977).

[26] **Mathew Robert Waugh**, "Characterization and Application of Transparent Conducting Thin Films", thesis is submitted in partial fulfillment of the requirements for the Degree of Doctor of Engineering (Chemistry). University College London (2011).

[27] **C. Salim**, "Propriétés des fenêtres optiques ZnO:Al pour cellules solaires en couches minces à base de CIGS", thèse de doctorat, UNIVERSITE FERHAT ABBAS (SETIF), (19.12.2012).

[28] **A. Hakim, J. Hossain, K. A. Khan**, "Temperature effect on the electrical properties of undoped NiO thin films", Vol 34, Issue (12.12.2009).

[29] **Y. S. ZOU, H. P. Wang, S. L. Zhang**, "Structural, Electrical and Optical properties of Mg-doped $CuAlO_2$ films by pulsed laser deposition", View article online, RSCADV,4.41294, (2014).

[30] **Garnier**, "Elaboration de Couches Minces d'Oxydes Transparents et Conducteurs par Spray CVD Assiste par Radiation Infrarouge pour Applications Photovoltaïques", thèse de doctorat, l'Ecole Nat ionale Supérieure d'Arts et Métiers, (2009).

[31] **F. Simonis, M. van der Leij and C.J. Hoogendoorn**, "Solar Energy Mater", **1**. 221 (1979).

[32] **P. Drude**, Ann. Phys, 3 (1900) page 369.

[33] **E. Hecht**, "in Optics, 2nd edition, Addison-Wesley Publishing Company", Inc. (1990).

[34] **J.C. Manifacier, M. De Murcia, J.P. Fillard, E. Vicario**, "Thin Solid Films",41, 127 (1977).

[35] **J. Tauc, R. Grigorovici and A. Vancu**, "Phys. Status Solid", 15, 627 (1966).

[36] **N. Manjula, K. Usharani, A.R. Balu, V.S. Nagarethinam**, "Studies on the physical properties of three potentially important TCO thin films fabricated by a simplified spray technique under same deposition conditions", Int. J. Chem Tech Res. 6 (2014) 705–718.

[37] **Gracia M, Rojas F, Gordillo G**, "Morphological and optical characterization of SnO: F thin films deposited by spray pyrolysis. In: 20th European Photovoltaic Solar Energy Conference". Barcelona, Spain; (6–10 June 2005).

[38] **G. Haacke**, "New figure of merit for transparent conductors", J. Appl. Phys. 47 (1976) 4086–4089.

[39] **M. Batzill and U. Diebold**, "The surface and materials science of tin oxide", Prog. Surf. Sci. 79(2-4), 47–154 (2005).

[40] **E. Kohnke**, "Electrical and optical properties of natural stannic oxide crystals", Phys. Chem. Solids, 23, 1557-1562, (1962).

[41] **Reimann K. and Steube M**, "Experimental determination of the electronic band structureof SnO_2", Solid State Commun, 105, 649-652, (1998).

[42] **S. R. Shief**, "High pressure phases in SnO_2", 117 Gpa , Phys. Rev. B 73, 014105 (2006).

[43] **K. Von Rottkay, M. Rubin, Mater. Res. Soc. Symp. Proc**, "Optical indices of pyrolytic tin oxide glass", Vol. 10, p 426-449, (1966).

[44] **I. Guesmi**, "Dépôt de couches minces de cuivre sur substrats polymère de formes complexes par pulvérisation cathodique magnétron avec ionisation de la vapeur", thèse de doctorat, Université Paris Sud – XI, (2003).

[45] **F. J. YUSTA, M. L. HITCHMAN and S. H. SHAMLIAN**, "CVD preparation and characterization of tin dioxide films for electro chemical applications", J. Mater. Chem., vol7, p1421, (1997).

[46] A. **RAHAL**,"Elaboration des verres conducteurs par déposition de ZnO sur des verres ordinaires", Memoire de Magister , UNIVERSITE D'ELOUED, (2013).

[47] **W.R. Grove**, Phil. Trans. Roy.Soc. London, 142, 87 (1852).

[48] **O.Daranfad**, Mémoire de magister, Université de Constantine (2010) 14-24.

[49] **Trommer, R.M,** "Obtencao caracterizao de revestimentos de hidroxiapatita sobre substratos de aço inoxidavel 316L utilizando a técnica de deposiçao quamica de vapor assistida porchama. Master Thesis", Universidade Federal do Rio Grande do Sul, Brazil (2006).

[50] **A.R. West**, "Solid State Chemistry", John willey & Sons, Singapore, (2003).

[51] **K. L. Chopra**, "Thin Film Phenomena", McGraw Hill, New York (1969).

[52] **L. D. Smith**, "Thin-Film Deposition Principles & Practice", McGraw-Hill: New York, (1995), pp.1-7.

[53] **K. Gelin; A. Roos; F. Geotti-Bianchini; P. v. Nijnatten**, "Optical Materials", (**2005),** 27. (4), 705-712.

[54] **R.A.Stradling**, "Growth and Characterisation of Semiconductors". IOP Publishing Ltd: New York, (1990), 17-35.

[55] **Kresge, C. T. Leonowicz, M. E. Roth, W. J. Vartuli,** J. C. Beck, J. S, Nature(**1992),** 359, 710.

[56] **Zeng. Acosta, R.E, Romankiw, L.T, VonGutfeld, R. J**, "Sol Thin Films", 95 (1982),131.

[57] **B. A. Movchan and A. V. Demchishin**, "Study of the Structure and Properties of Dioxide thin, Fiz. Met. Metalloved", Vol. 28, (1969), 83-90.

[58] **Behrisch. R**, "Sputtering by Particle Bombardment", Springer, Berlin (1981).

[59] **Vesna Zagreb, Croatia**, "Mesoporous Transparent Conducting Films of Antimony Doped Tin Oxide as Nanostructured Electrodes", Universitat München, (2013).

[60] **B. Wang, Y.N. Zhao, Z. He**, "The effects of deposition parameters on the crystallographic orientation of AIN films prepared by RF reactive sputtering", Vacuum. Vol. 48, (1997) 427-429.

[61] **L . B. FREUND, S . SURESH**, "Thin Film Materials Stress ", Defect Formation andSurface Evolution Cambridge University, (2003).

[62] **J. R. Creighton and P. Ho,**"Introduction to Chemical Vapor Deposition (CVD) ", Sandia National Laboratories P.O. Box 5800, MS0601 Albuquerque, NM 87185-0601, (2001).

[63] **K. L. Chopra**, "Thin Film Phenomena", McGraw Hill, New York (1969).

[64] **P. Kirk and R Pillar**, "The deformation response of sol-gel-derived thin films Mater". Sci, Vol. 34, 16, 3967-3975, (1999).

[65] Chemistry of sol gel science, Sogang university, Page 2, Vol 29.

[66] **K.L. Choy**, "Chemical vapor deposition of coatings, Department of Materials", Prince Consort Road, London SW7 2BP, UK, Progress in Materials Science, (2003).

[67] **MILEA, C. BOGATU, A.DUTA1,** "THE INFLUENCE OF PARAMETERS IN SILICA SOL-GEL PROCESS", Bulletin of the Transilvania University of Brasov Series I: Engineering Sciences, Vol. 4 (53) No. 1, (2011).

[68] **A. Kopp Alves and al.**,"Novel Synthesis and Characterization of Nanostructured Materials", Engineering Materials, DOI: 10.1007/978-3-642-41275-2, Springer-Verlag Berlin Heidelberg (2013).

[69] **Perednis, D**, "Thin film deposition by spray pyrolysis and the application in solide oxide fuel cells", Ph.D. Thesis, Swiss Federal Institute of Technology Zurich (2003).

[70] **Choy, K.L. Su. B,** "Growth behavior and microstructure of CdS thin films deposited by an electrostatic spray assisted vapor deposition (ESAVD) process", Thin Solid Films 388, 9–14 (2001).

[71] **Anton Kock, Jordi Teva, Jochen Kraft, Jorg Siegert, and Franz Schrank**, "Modeling Spray Pyrolysis Deposition", Proceedings of the World Congress on Engineering, London, U.K. WCE, 3 – 5 July (2013).

[72] **A. Nakaruk and C. Sorrell**, "Conceptual model for spray pyrolysis mechanism: fabrication and annealing of titania thin films", Journal of Coatings Technology and Research, vol. 7, no. 5, pp. 665–676, (2010).

[73] **Sonia R. Sousa PhD,** "**UV-VIS Spectroscopy - Chemical Analysis** Solutions Unit", Marketing Manager – Spectroscopy, (21 January 2009).

[74] **F. HADJERSI** ,"Investigation des propriétés structurales, optiques et électriques des films ITO élaborés par pulvérisation cathodique RF; Effet du recuit" , Université Ferhat Abbas de Sétif , (2011).

[75] **M. Rand**, "Spectrophotometric Thickness Measurement for Very Thin SiO_2 Films on Si, Journal of Applied Physics", Volume 41, Number 2, (1970).

[76] **R. JURGEN , M. ARENDT**, "Introduction to Classical and Modern Optics" , Fourth edition , Published by Prentice-Hall Inc , (1995).

[77] **C. S. WILIAMS, O. BECKLUND,** "Optics: A Short Course for Engineers and Scientists" , John Wiley et sons , (1972).

[78] **T. GUNGOR , H. TOLUNAY**, "Drift mobility measurements in a-SiN_x:H ", Journal of Non- Crystalline Solids, vol 282 , p197-202, (2001).

[79] **F.Urbach**, Phys. Rev. 92, 1324 (1953).

[80] **Natsume Y, Sakata H, Hirayama T**, "Low temperature electrical conductivity and optical absorption edge of ZnO films prepared by chemical vapor deposition". Phys Stat Sol (A), (1995),148:485–95.

[81] **Schroder, Dieter K**, "Semiconductor Material and Device Characterization", John Wiley & Sons, Inc, (1998).

[82] **A. Benhaoua, A. Rahal** , **B. Benhaoua, M. Jlassi**, "Effect of fluorine doping on the structural, optical and electrical properties of SnO_2 thin films prepared by spray ultrasonic", Vol. 70, p. 61-69, (2014).

[83] **B. D. Cullity,** "Elements of X-ray Diffraction", Addison Wesley, Massachusetts (1956).

[84] **H. P. Klug and L. E. Alexander**, "X-ray Diffraction Procedures", Wiley, New York, (1954).

[85] **A. BOULLE**, "Two-dimensionnal XRD profile modelling in Imperfect Epitaxial Layers", Diffraction Analysis of the Microstructure of Materials Springer Series in Materials Science Vol 68 , p505-526, (2004).

[86] **I. Boudraa**, "Synthèse et étude structurale par diffraction des rayons X des phosphates mixte des métaux à valence II,III et V", thèse de Magister, Université Mentourie , Algérie, (2010) .

[87] **C. Marcel, N. Naghavi**, G. Couturier, J. Salardenne, J.M. Tarascon, J. Appl. Phys. 91 (2002) 4291.

[88] **B.D. Cullity**, "Elements of X-Ray Diffraction", 2nd ed., Addison – Wesley publishing company Inc., Philippines, (1978). vol. 99 (Printed in U.S.A.).

[89] **A.V. Moholkar, S.M. Pawar, K.Y. Rajpure, S.N. Almari, P.S. Patil, C.H. Bhosale**, "Solar energy mater", Solar Cells 92 (2008) 1439.

[90] **Y. Wang, J. Ma, Feng Ji, Xuhu Yu, Honglei Ma**, "Structural and photoluminescence characters of SnO:Sb films deposited by RF magnetron sputtering", J. Lumin. 114 (2005) 71–76.

[91] **P.S. Shewale, Kyu Ung Sim, Ye-bin Kim, J.H. Kim, A.V. Moholkar, M.D. Uplane**, "Structural and photoluminescence characterization of SnO_2: F thin films deposited by advanced spray pyrolysis technique at low substrate temperature", J. of Luminescence 139 (2013) 113–118.

Abstract

The object of this present work is to obtain conducting transparent SnO_2 thin films deposited by spray pyrolysis technique (home made) on glass substrates heated at 480 ^{0}C with different percentage of Antimony (Sb) dopant Our interest is on the investigation of the doping level influence on the optical, structural and electrical properties of SnO_2 thin films elaborated in our laboratory (VTRS: Valorsation et Technologie de Resources Sahariennes). We have used as precursor source source $SnCl_3$ and $SbCl_3$ as dopant. We varied the rate of doping from 0 to 1% in the starting solution.

X-ray diffraction patterns confirm that films are rutile structure and exhibit the (211) direction as a preferred orientation with low energy of formation. The optical characterization of deposited films was carried out using UV-Vis spectrometry in the spectral range 300-900 nm. The analysis of the transmittance spectra allows us to deduce that the films thicknesses, value of the transmittance and optical band gaps were affected by the amount of dopant. Hence, the average value of the transmittance is around 85%, the values of the gap were found between 3.65 and 3.92 eV, The four points technique showed that all thin films have as resistance sheet range [31.07- 806 (Ω.cm^{-2})].

***Key Words*:** thin films, Tin dioxide, Antimony, Electrical conductivity, transmittance, X-ray diffraction.

Résumé

Dans ce travail, nous avons élaboré des couches minces de à partir d'une source de dissoute dans du Méthanol avec différents pourcentage de dopage en Antimoine (Sb) utilisant comme source de dopant ($SbCl_3$). L'objet de ce travail est d'étudier l'influence de ce dopage sur les caractéristiques optiques, structurelles et électrique du SnO_2. Ces couches sont élaborées par la technique de spray pyrolysis sur des substrats en verre chauffés à une température donnée (480^{0}C).

La caractérisation structurale des couches par analyse de diffraction des rayons X a montré que les couches sont de structure quadrique rutile. avec une orientation préférentielle (211) qui est de faible énergie de croissance. La caractérisation optique des films a été réalisée à l'aide spectrométrie UV- Visible dans la gamme spectrale allant de 300 à 900 nm, et elle a montré que les films sont transparents avec une valeur moyenne de la transmittance de l'ordre de 85 % dans le visible, ainsi, cette technique nous a permis de déterminer les épaisseurs des couches élaborées, la variation de l'énergie du gap optique E en fonction du dopage en : est de 3.65 à 3.92 eV, La technique de quatre points a montré que les couches de ont une résistance carré allant de 31.07 à 806 (Ω.cm^{-2})**.**

***Mots clés*:** Couche mince, Dioxyde d'étain, Antimoine, Conductivité électrique, Transmittance, diffraction des rayons X.